STAR★METHODS

KEY RESOURCES TABLE

REAGENT or RESOURCE	SOURCE	IDENTIFIER
Antibodies		
AGO2	Wako	Cat#011-22033
Beta actin	AbCam	Cat#ab8227
CAPRIN1	Protein Tech Group	Cat#15112-1-AP
DDX6	Bethyl Labs	Cat#A300-461A
EDC4	Santa Cruz	Cat#sc-8418
EIF3B	Santa Cruz	Cat#sc-16377
EIF4G	Santa Cruz	Cat#sc-11373
FMR1	Protein Tech Group	Cat#13755-1-AP
FMR1	Santa Cruz	Cat#sc-101048
FXR1	Santa Cruz	Cat#sc-10554
FXR1	Bethyl Labs	Cat#A303-892A
FXR1	Protein Tech Group	Cat#13194-1-AP
FXR2	Santa Cruz	Cat#sc-32266
G3BP1	Santa Cruz	Cat#sc-365338
G3BP1	AbCam	Cat#ab86135
G3BP2	AbCam	Cat#ab86135
GFP	Rockland	Cat#600-901-215
Goat anti-mouse AlexaFluor546	Life Technologies	Cat#A-20183
Goat Anti-Mouse IgG (H+L)	Jackson	Cat#115-035-062
Goat anti-rabbit AlexaFluor488	Life Technologies	Cat#A-11008
Goat Anti-Rabbit IgG (H+L)	Jackson	Cat#115-035-144
mCherry	Clontech	Cat#632543
NUFIP2	Bethyl Labs	Cat#A301-600A
NUFIP2	Protein Tech Group	Cat#17752-1-AP
PABPC1	Santa Cruz	Cat#sc-32318
RPS6	Santa Cruz	Cat#sc-13007
TIA1	Santa Cruz	Cat#sc-1751
UBAP2	Bethyl Labs	Cat#A304-626A
UBAP2	Bethyl Labs	Cat#A304-627A
UBAP2L	Bethyl Labs	Cat#A300-534A
UBAP2L	Bethyl Labs	Cat#A300-533A
USP10	Bethyl Labs	Cat#A300-900A
USP10	Bethyl Labs	Cat#A300-901A
Chemicals, Peptides, and Recombinant Proteins		
5′-Cy5-Oligo d(T)20	Gene Link	Cat#26-4420-02
Actinomycin D	Sigma	Cat#A5156-1VL
Chromotek-GFP-Trap Beads	Bulldog Bio	Cat#GTA020
Fetal Bovine Serum, Premium, Heat-Inactivated	Atlanta Biologicals	Cat#S11150H
G3BP1 recombinant protein	Novus	Cat#NBP1-50925-50UG
G3BP2 recombinant protein	Novus	Cat#NBP1-78843-100UG
GIBCO DMEM, High Glucose, Pyruvate	Thermo Fisher Scientific	Cat#11995065
GIBCO Opti-MEM Reduced Serum Medium	Thermo Fisher Scientific	Cat#31985062
GIBCO Penicillin-Streptomycin (10,000 U/mL)	Thermo Fisher Scientific	Cat#15140122

(*Continued on next page*)

Continued

REAGENT or RESOURCE	SOURCE	IDENTIFIER
HALT phosphatase inhibitors (Pierce)	Thermo Fisher	Cat#78420
In-Fusion HD Cloning Plus	Takara Bio	Cat#638910
Lipofectamine 3000 Transfection Reagent	Thermo Fisher Scientific	Cat#L3000008
Paraformaldehyde (16%)	Electron Microscopy Services	Cat#15710
Phusion® High-Fidelity DNA Polymerase	New England Biolabs	Cat#M0530L
Protease inhibitor tablets (EDTA-free)	Sigma	Cat#4693132001
Quick Ligase	NEB	Cat#M2200
RNase Cocktail Enzyme Mix (RNase A, RNase T1)	Thermo Fisher	Cat#AM2286
Sodium arsenite	Sigma	Cat#S7400-100G
TURBO™ DNase (2 U/μL)	Thermo Fisher	Cat#AM2238
Experimental Models: Cell Lines		
Human: HeLa	ATCC	Cat#ATCC CCL-2
Human: HEK293T	Marc Diamond, UTSW	N/A
Human: HEK293	Marc Diamond, UTSW	N/A
Human: U2OS WT	Kedersha et al., 2016	N/A
Human: U2OS WT Tet Repressor	Kedersha et al., 2016	N/A
Human: U2OS G3BP1/G3BP2 2KO	Kedersha et al., 2016	N/A
Human: U2OS CAPRIN1 KO	Kedersha et al., 2016	N/A
Human: U2OS G3BP1/G3BP2/CAPRIN1 3KO	This paper	N/A
Human: U2OS USP10 KO	This paper	N/A
Human: U2OS G3BP1/G3BP2/USP10 3KO	This paper	N/A
Human: U2OS FXR2 KO	This paper	N/A
Human: U2OS FXR1/FXR2/FMR1 3KO	This paper	N/A
Human: U2OS NUFIP2 KO	This paper	N/A
Human: U2OS FXR1/FXR2/FMR1/NUFIP2 4KO	This paper	N/A
Human: U2OS UBAP2L KO	This paper	N/A
Human: U2OS UBAP2/2L 2KO	This paper	N/A
Oligonucleotides		
NUFIP2 gRNA targeting sequence: ATCATCAAGTCGCTTATCCC	This paper	N/A
FMR1 gRNA targeting sequence: AAGAGGCGGCACATAAGGAT	This paper	N/A
FXR1 gRNA targeting sequence: TTCCTAGGAATCTCGTTGGT	This paper	N/A
FXR2 gRNA targeting sequence: CCCCATAGG TTCGAGTCGCA	This paper	N/A
CAPRIN1 gRNA targeting sequence: CTCCCGGAGGAACCCGACGG	This paper	N/A
USP10 gRNA targeting sequence: CTCCCGGAGGAACCCGACGG	This paper	N/A
UBAP2L gRNA targeting sequence: CTCCCGGAGGAACCCGACGG	This paper	N/A
UBAP2 gRNA targeting sequence: TTTCCCGAGCACCTCGACAA	This paper	N/A
UBAP2 gRNA targeting sequence: TGAGACGGAGGTCGCTGCCG	This paper	N/A
UBAP2 gRNA targeting sequence: GTTCGCGGTGTTCATGCTAC	This paper	N/A
UBAP2 gRNA targeting sequence: GTGAGCAGTGACCATTGTCG	This paper	N/A
UBAP2 gRNA targeting sequence: GTCTCAAGTTCCGCATCCTC	This paper	N/A
UBAP2 gRNA targeting sequence: GCCGCGCCCTTGGTGACCTC	This paper	N/A
NonTarget gRNA targeting sequence: ACGGAGGCTAAGCGTCGCAA	This paper	N/A
Recombinant DNA		
FM5-CAPRIN1-mCherry	This paper	N/A
FM5-CAPRIN1-mGFP	This paper	N/A

(*Continued on next page*)

Continued

REAGENT or RESOURCE	SOURCE	IDENTIFIER
FM5-CAPRIN1-miRFP670	This paper	N/A
FM5-DCP1A-mCherry	This paper	N/A
FM5-EIF3F-mCherry	This paper	N/A
FM5-FUSΔNLS (1-513)-mGFP	This paper	N/A
FM5-G3BP1 IDR1/2-mGFP	This paper	N/A
FM5-G3BP1-mCherry	This paper	N/A
FM5-G3BP1-miRFP670	This paper	N/A
FM5-HNRNPA1 ΔNLS-mCherry	This paper	N/A
FM5-HNRNPA1 ΔNLS-mGFP	This paper	N/A
FM5-iLID-mGFP	This paper	N/A
FM5-iLID-mGFP-Fe	This paper	N/A
FM5-iLID-mGFP-G3BP1ΔNTF2	This paper	N/A
FM5-mCherry	Marc Diamond, UTSW	N/A
FM5-mCherry-CAPRIN1	This paper	N/A
FM5-mCherry-FXR1	This paper	N/A
FM5-mCherry-G3BP1	This paper	N/A
FM5-mCherry-UBAP2L	This paper	N/A
FM5-mCherry-USP10	This paper	N/A
FM5-mCherry-USP10 NIMx1 (1-33)	This paper	N/A
FM5-mCherry-USP10 NIMx2 (1-33x2)	This paper	N/A
FM5-mGFP	This paper	N/A
FM5-mGFP-CAPRIN1	This paper	N/A
FM5-mGFP-CAPRIN1 1-359	This paper	N/A
FM5-mGFP-CAPRIN1 1-381	This paper	N/A
FM5-mGFP-CAPRIN1 1-604	This paper	N/A
FM5-mGFP-CAPRIN1 252-709	This paper	N/A
FM5-mGFP-CAPRIN1 382-604	This paper	N/A
FM5-mGFP-CAPRIN1 382-709	This paper	N/A
FM5-mGFP-CIRBP	This paper	N/A
FM5-mGFP-DCP1A	This paper	N/A
FM5-mGFP-DDX3X	This paper	N/A
FM5-mGFP-DDX6	This paper	N/A
FM5-mGFP-EDC3	This paper	N/A
FM5-mGFP-EIF3F	This paper	N/A
FM5-mGFP-ELAVL1	This paper	N/A
FM5-mGFP-FKBP DimerD-G3BP1 ΔNTF2	This paper	N/A
FM5-mGFP-FMR1	This paper	N/A
FM5-mGFP-FUSΔNLS (1-513)	This paper	N/A
FM5-mGFP-FXR1	This paper	N/A
FM5-mGFP-G3BP1	This paper	N/A
FM5-mGFP-G3BP1 F33W	This paper	N/A
FM5-mGFP-G3BP1 RBD SWAP-CAPRIN1	This paper	N/A
FM5-mGFP-G3BP1 RBD SWAP-FUS	This paper	N/A
FM5-mGFP-G3BP1 RBD SWAP-FXR1	This paper	N/A
FM5-mGFP-G3BP1 RBD SWAP-HNRNPA1	This paper	N/A
FM5-mGFP-G3BP1 RBD SWAP-TIA1	This paper	N/A
FM5-mGFP-G3BP1 RBD SWAP-UBAP2L	This paper	N/A
FM5-mGFP-G3BP1 S38F	This paper	N/A

(*Continued on next page*)

Continued

REAGENT or RESOURCE	SOURCE	IDENTIFIER
FM5-mGFP-G3BP1ΔIDR1	This paper	N/A
FM5-mGFP-G3BP1ΔIDR1/2	This paper	N/A
FM5-mGFP-G3BP1ΔIDR2	This paper	N/A
FM5-mGFP-G3BP1ΔNTF2	This paper	N/A
FM5-mGFP-G3BP1ΔRBD	This paper	N/A
FM5-mGFP-G3BP1ΔRGG	This paper	N/A
FM5-mGFP-G3BP1ΔRRM	This paper	N/A
FM5-mGFP-G3BP2A	This paper	N/A
FM5-mGFP-G3BP2B	This paper	N/A
FM5-mGFP-HNRNPA1ΔNLS	This paper	N/A
FM5-mGFP-LSM14A	This paper	N/A
FM5-mGFP-NUFIP2	This paper	N/A
FM5-mGFP-OTUD4	This paper	N/A
FM5-mGFP-PABPC1	This paper	N/A
FM5-mGFP-TDP43 C35 (85-414)	This paper	N/A
FM5-mGFP-TIA1	This paper	N/A
FM5-mGFP-TIAR	This paper	N/A
FM5-mGFP-UBAP2L	This paper	N/A
FM5-mGFP-UBAP2L 1-527	This paper	N/A
FM5-mGFP-UBAP2L 1-780	This paper	N/A
FM5-mGFP-UBAP2L 291-1087	This paper	N/A
FM5-mGFP-UBAP2L 467-540	This paper	N/A
FM5-mGFP-UBAP2L 528-1087	This paper	N/A
FM5-mGFP-UBAP2L 91-1087	This paper	N/A
FM5-mGFP-USP10	This paper	N/A
FM5-mGFP-USP10 NIMx1 (1-33)	This paper	N/A
FM5-mGFP-USP10 NIMx2 (1-33x2)	This paper	N/A
FM5-mGFP-YBX1	This paper	N/A
FM5-miRFP670-FXR1	This paper	N/A
FM5-miRFP670-G3BP1	This paper	N/A
FM5-miRFP670-UBAP2L	This paper	N/A
FM5-PABPC1-EYFP	Marc Diamond, UTSW	N/A
FM5-sspB-mCherry	This paper	N/A
FM5-sspB-mCherry-CAPRIN1 1-359	This paper	N/A
FM5-sspB-mCherry-CAPRIN1 1-381	This paper	N/A
FM5-sspB-mCherry-CAPRIN1 1-604	This paper	N/A
FM5-sspB-mCherry-CAPRIN1 132-251	This paper	N/A
FM5-sspB-mCherry-CAPRIN1 382-604	This paper	N/A
FM5-sspB-mCherry-CAPRIN1 382-709	This paper	N/A
FM5-sspB-mCherry-CAPRIN1 RBD (605-709)	This paper	N/A
FM5-sspB-mCherry-CIRBP	This paper	N/A
FM5-sspB-mCherry-DCP1A	This paper	N/A
FM5-sspB-mCherry-EDC3	This paper	N/A
FM5-sspB-mCherry-EIF3F	This paper	N/A
FM5-sspB-mCherry-FUS RBD	This paper	N/A
FM5-sspB-mCherry-FXR1 RBD	This paper	N/A
FM5-sspB-mCherry-G3BP1 IDR1-RBD	This paper	N/A
FM5-sspB-mCherry-G3BP1 IDR1/2	This paper	N/A

(*Continued on next page*)

Continued

REAGENT or RESOURCE	SOURCE	IDENTIFIER
FM5-sspB-mCherry-G3BP1 IDR1/2-CAPRIN1 RBD	This paper	N/A
FM5-sspB-mCherry-G3BP1 IDR1/2-CAPRIN1 RBD Scrambled	This paper	N/A
FM5-sspB-mCherry-G3BP1 IDR1/2-DDX3X RGG	This paper	N/A
FM5-sspB-mCherry-G3BP1 IDR1/2-FMR1 RGG	This paper	N/A
FM5-sspB-mCherry-G3BP1 IDR1/2-FUS IDR	This paper	N/A
FM5-sspB-mCherry-G3BP1 IDR1/2-FUS RBD	This paper	N/A
FM5-sspB-mCherry-G3BP1 IDR1/2-FXR1 RBD	This paper	N/A
FM5-sspB-mCherry-G3BP1 IDR1/2-FXR1 RGG	This paper	N/A
FM5-sspB-mCherry-G3BP1 IDR1/2-HNRNPA1 RBD	This paper	N/A
FM5-sspB-mCherry-G3BP1 IDR1/2-LSM14A RBD	This paper	N/A
FM5-sspB-mCherry-G3BP1 IDR1/2-MAPT MT	This paper	N/A
FM5-sspB-mCherry-G3BP1 IDR1/2-PAB1 RBD	This paper	N/A
FM5-sspB-mCherry-G3BP1 IDR1/2-RGG	This paper	N/A
FM5-sspB-mCherry-G3BP1 IDR1/2-TIA1 RBD	This paper	N/A
FM5-sspB-mCherry-G3BP1 IDR1/2-UBAP2L RBD	This paper	N/A
FM5-sspB-mCherry-G3BP1 RBD	This paper	N/A
FM5-sspB-mCherry-G3BP1ΔNTF2	This paper	N/A
FM5-sspB-mCherry-G3BP1ΔNTF2/ΔIDR2	This paper	N/A
FM5-sspB-mCherry-G3BP2AΔNTF2	This paper	N/A
FM5-sspB-mCherry-G3BP2BΔNTF2	This paper	N/A
FM5-sspB-mCherry-HNRNPA1 RBD	This paper	N/A
FM5-sspB-mCherry-TIA1 RRMx1	This paper	N/A
FM5-sspB-mCherry-TIA1 RRMx2	This paper	N/A
FM5-sspB-mCherry-TIA1 RRMx3 (RBD)	This paper	N/A
FM5-sspB-mCherry-UBAP2L 1-90	This paper	N/A
FM5-sspB-mCherry-UBAP2L 124-204	This paper	N/A
FM5-sspB-mCherry-UBAP2L 239-290	This paper	N/A
FM5-sspB-mCherry-UBAP2L 291-494	This paper	N/A
FM5-sspB-mCherry-UBAP2L 467-540	This paper	N/A
FM5-sspB-mCherry-UBAP2L 495-527	This paper	N/A
FM5-sspB-mCherry-UBAP2L 528-780	This paper	N/A
FM5-sspB-mCherry-UBAP2L 781-1087	This paper	N/A
FM5-sspB-mCherry-UBAP2L RBD (124-290)	This paper	N/A
FM5-sspB-mCherry-USP10	This paper	N/A
FM5-sspB-mCherry-YBX1	This paper	N/A
FM5-UBAP2L-mGFP	This paper	N/A
FM5-USP10-mGFP	This paper	N/A
FM5-USP10-mCherry	This paper	N/A
FM5-USP10-miRFP670	This paper	N/A
FM5-YBX1-mCherry	This paper	N/A
FM5-YBX1-mGFP	This paper	N/A
p-mCherry-G3BP1-C1	Kedersha et al., 2016	N/A
pCas-Guide	Origene	Cat#GE100002
pcDNA4 t/o-GFP-G3BP1 F33W	Kedersha et al., 2016	*N/A*
pcDNA4 t/o-GFP-G3BP1 S38F	This paper	N/A
pcDNA4 t/o-GFP-G3BP1 WT	Kedersha et al., 2016	N/A
pcDNA4 t/o-GFP-NES	This paper	N/A
pcDNA4 t/o-GFP-UBAP2L	This paper	N/A

(*Continued on next page*)

Continued

REAGENT or RESOURCE	SOURCE	IDENTIFIER
pCRISPRv2	Shalem et al., 2014	N/A
pGEM®-T Easy vector	Promega	Cat#A137A
pHR-FUS IDR-mCherry-sspB	Bracha et al., 2018	N/A
pHR-G3BP1 NTF2-IDR1-mCherry-sspB	This paper	N/A
pHR-G3BP1 NTF2-mCherry-sspB	This paper	N/A
pHR-G3BP1ΔRBD-mCherry-sspB	This paper	N/A
pHR-G3BP1ΔRGG-mCherry-sspB	This paper	N/A
pHR-G3BP1-mCherry-sspB	This paper	N/A
pHR-mCherry-sspB	Bracha et al., 2018	N/A
pHR-sspB-mCherry-G3BP1 IDR1	This paper	N/A
pHR-sspB-mCherry-G3BP1 IDR1/2	This paper	N/A
pHR-sspB-mCherry-G3BP1 IDR1/2-RRM	This paper	N/A
pHR-sspB-mCherry-G3BP1 IDR2	This paper	N/A
pHR-sspB-mCherry-G3BP1 IDR2-RBD	This paper	N/A
pHR-sspB-mCherry-G3BP1 IDR2-RRM	This paper	N/A
pHR-sspB-mCherry-G3BP1 RBD	This paper	N/A
pHR-sspB-mCherry-G3BP1 RGG	This paper	N/A
pHR-sspB-mCherry-G3BP1 RRM	This paper	N/A
pHR-sspB-mCherry-sspB	This paper	N/A
PSP	Marc Diamond, UTSW	N/A
VSVG	Marc Diamond, UTSW	N/A
Software and Algorithms		
ImageJ	NIH	https://imagej.nih.gov/ij/
MATLAB	MathWorks	https://www.mathworks.com/products/MATLAB.html

LEAD CONTACT AND MATERIALS AVAILABILITY

Further information and requests for resources and reagents should be directed to and will be fulfilled by the lead contact, Clifford P. Brangwynne (cbrangwy@princeton.edu). All reagents generated in this study will be made available on request, but we may require a payment and/or a completed Materials Transfer Agreement if there is potential for commercial application.

EXPERIMENTAL MODEL AND SUBJECT DETAILS

Cells were cultured in DMEM (GIBCO) with 10% FBS (Atlanta Biological), supplemented with 1% streptomycin and penicillin, and kept in a humidified incubator at 37°C with 5% CO_2. All cell lines tested mycoplasma-negative. HEK293 and HEK293T (immortalized human female kidney-derived cells) were kind gifts from Marc Diamond lab (UT Southwestern). HeLa (immortalized human female cervical cancer-derived cells) were obtained from ATCC. U2OS cells (human female osteosarcoma cells) and U2OS G3BP1/2 (''G3BP'') knockout (KO) cells were previously described (Kedersha et al., 2016). G3BP KO was confirmed independently in by western blot (Figure S1B). Details regarding additional described U2OS knockout cell lines are provided in Table S2. All cell lines are adherent to plastic/glass substrates and divide (double) every 24 h, on average. ''Confluency'' refers to the state when cells completely cover the bottom of dish, and hence stop dividing. Thus, when methods state 1:8 dilution (''passage'' into new dish), ~72 h will be required to reach next confluency.

METHOD DETAILS

Plasmid construction

Unless indicated (e.g., pHR lentiviral vector, SFFV promoter), all lentiviral DNA plasmids were generated using the FM5 lentiviral vector (kind gift from Marc Diamond lab, UT Southwestern), which features the Ubiquitin C promoter. DNA fragments encoding our proteins of interest were amplified by PCR with Phusion® High-Fidelity DNA Polymerase (NEB). Oligonucleotides used for

PCR were synthesized by IDT. In-Fusion HD cloning kit (Takara) was used to insert the PCR amplified fragments into the desired linearized vector, which featured standardized linkers and overlaps to allow cloning in high throughput. Plasmid inserts were confirmed by GENEWIZ Sanger sequencing, reading from both ends of the insert. For all sspB-mCherry-tagged DNA constructs, correct sequencing was confirmed a second time by an independent researcher. Stress granule (SG) rescue defects associated with the G3BP S38F mutant were confirmed using two different fully sequenced DNA constructs (FM5-mGFP-G3BP1 S38F and pcDNA4 t/o-GFP-G3BP1 S38F) tested by two separate labs.

Generation of lentivirus and lentiviral transduction

All live cell imaging experiments were performed using cells stably transduced with lentivirus, with the exception of light-induced sspB-/iLID-ΔNTF2 dimer-mediated rescue of G3BP knockout (Figure S1J; see Transient transfection). Lentiviruses containing desired constructs were produced using a previously optimized protocol (Sanders et al., 2014) by transfecting the plasmid along with helper plasmids VSVG and PSP (kind gift from Marc Diamond lab, UT Southwestern) into HEK293T cells with Lipofectamine™ 3000 (Invitrogen). Virus was collected 2-3 days after transfection and used to infect WT U2OS or G3BP KO U2OS cells. Lentivirus transduction was performed in 96-well plates. Three days following lentivirus application to cells at low confluency, cells were passaged for stable maintenance or directly to 96-well fibronectin-coated glass bottom dishes for live cell microscopy. For non-Corelet experiments, stable cell lines were passaged at least 3-times over 8+ days prior to use in live cell imaging experiments to eliminate cells expressing lethal levels of the fusion protein of interest. In all experiments, 90%+ of cells featured expression of the protein of interest at a range of concentrations (typically < 5 μM; estimated concentrations are noted as relevant in the figure legends). This specific protocol was designed to avoid artifact-prone concentrations of fusion proteins that can occur with lipid-based transient transfection, which has previously been shown to induce interferon signaling and stress granule formation (e.g., GFP transfection of WT U2OS cells can lead to stress granules in ~20% of cells) (Guo et al., 2019; Hagen et al., 2015; Panas et al., 2019; Tourrière et al., 2003).

Transient transfection

Unlike all other experiments (see above), light-induced (sspB/iLID) ΔNTF2 dimer-mediated rescue of G3BP knockout was performed using transient transfection (Figure S1J). Initial attempts to rescue defects (data not shown) using lentivirus mediated stable expression were not successful due to inability to reach sufficiently high concentrations of the individual fusion proteins (i.e., > 8 μM of both mCherry-sspB-G3BP1ΔNTF2 and mGFP-iLID-G3BP1ΔNTF2). See Figure 1L for constitutive dimer mGFP-FKBP-G3BPΔNTF2, data collected using stable, lentivirus-mediated expression. Thus, individual wells of a 96-well plate containing G3BP1/2 KO U2OS cells were transfected with both mCherry-sspB-G3BP1ΔNTF2 and mGFP-iLID-G3BP1ΔNTF2 using Lipofectamine™ 3000 (Invitrogen) according to manufacturer's recommendations. 18 h later, cells were observed to feature both fusion proteins diffusely expressed throughout the cytoplasm. Arsenite was added to a final concentration of 400 μM. 1 h later, cells were imaged. Three biological replicates were performed. In rare cells with very high concentrations of both components (> 10 μM of each) **(**Figure S1J**)**, stress granules were observed, regardless of time of blue light activation. The light-independent nature of dimer-based rescue at these concentrations is consistent with the measured *in vitro* dark state K_d of 4.3 μM for iLID-sspB (Guntas et al., 2015). At such concentrations, iLID and sspB are expected to interact strongly in the dark. The *in vitro* light state K_d for iLID-sspB of 0.2 μM for iLID-sspB (or ~10 nM for "core" measurements, see Phase diagram data collection), which sets the lower limit for the assay.

Microinjections into live U2OS cells

Microinjections were performed using an Eppendorf Femtojet microinjector mounted on an Axiovert 200M Widefield at 60x magnification. Microneedles were pulled from borosilicate glass with O.D. 1 mm and I.D. 0.78 mm using Sutter Instrument Model P-97. U2OS WT cells stably expressing GFP-CAPRIN1 (~1-2 μM) were plated on 35 mm glass bottom dishes (MatTek) in DMEM (GIBCO) with 10% FBS (Atlanta Biological), supplemented with 1% streptomycin and penicillin, and kept in a humidified incubator at 37°C and 5% CO2. Prior to injection, media was replaced with fresh media supplemented with 10 mM HEPES to buffer against pH changes during CO_2-free microinjection (Maharana et al., 2018). DNase (TURBO from Thermo Fisher, 2 U/μL), RNase (Cocktail Enzyme Mix from Thermo Fisher featuring RNase A: 0.5 U/μL, RNase T1: 20 U/μL), or buffer control were diluted 1:8 in TAMRA dye/PBS and injected directly into the cytoplasm with a pressure of 30 hPa for as short a time as possible. For each trial, approximately 100-150 cells were individually injected. Media was exchanged for fresh media containing 400 μM arsenite to induce polysome disassembly ("RNA influx"). 45-60 min later, cells were imaged with a Nikon A1 laser scanning microscope. Fields of view with TAMRA-positive cells were identified using the 546 laser-line in the absence of 488 to avoid potential bias with respect to cell selection. Upon finding cells, images were taken with both 488 and 546 laser lines and cells were scored for presence or lack of stress granules, measuring the TAMRA fluorescence in the cytoplasm (arbitrary units).

Live cell confocal microscopy

Cells were imaged on fibronectin-coated 96-well glass bottom dishes (Cellvis). Confocal images were taken on a Nikon A1 laser scanning confocal microscope using a 60x oil immersion lens with a numerical aperture of 1.4. The microscope stage was equipped with a humidified incubator to keep cells at 37°C and 5% CO_2. Proteins tagged with mCherry, mGFP ("GFP"), EYFP, and miRFP670 ("iRFP") were imaged with 560, 488, 488, and 640 nm lasers, respectively. All experiments and image acquisitions were performed on

living cells to avoid potential artifacts due to fixation, with three exceptions: (A) RNA-FISH experiments; (B) immunofluorescence studies; (C) Corelet/GFP co-localization analysis. No measurements of protein concentration were performed in fixed cells, as fluorescence intensity of proteins in specific cellular compartments were differentially affected by paraformaldehyde fixation. The above details apply to all imaging data in the manuscript with the exception of STED super-resolution (Figure 6G) and widefield microscopy (Figures 6H; S6H) images. See below for details.

Stimulated emission depletion (STED) super-resolution microscopy

For images shown in Figure 6G, G3BP KO cells stably expressing either iRFP-G3BP1 or mGFP-G3BP1 and iRFP-FXR1—in all cases at ~1-2 μM—were treated with 400 μM arsenite (1 h, humidified incubator) then imaged on an Abberior Instruments expert line STED laser scanning confocal microscope at 37°C. For single channel STED images, sequential image sets (each line imaged concurrently with and without the STED laser to control for bleaching artifacts) were taken with increasing STED power using the 'Custom Axis' options available in Imspector. For dual channel STED images, two sequential image sets were taken with each line imaging mGFP (+/− STED) and miRFP (+/− STED) with the first mGFP STED power set to 0% to avoid miRFP image bleaching, which occurred during the second image (again using the 'custom axis' option available in Imspector).

Widefield microscopy

For images displayed in Figure 6H and Figure S6H, G3BP KO or UBAP2L KO U2OS cells stably expressing GFP-UBAP2L were grown on glass coverslips, stressed with 400 μM arsenite when indicated, and fixed using 4% paraformaldehyde in PBS for 15-min, followed by 5-min post-fixation/permeabilization in ice cold methanol. Cells were blocked in 5% horse serum/PBS, and primary and secondary antibody incubations were performed in blocking buffer for 1 h with rocking. Following washes with PBS, cells were mounted in polyvinyl mounting media and imaged. Images were captured using a Nikon Eclipse E800 microscope with a 63x Plan Apo objective lens (NA 1.4) and illuminated with a mercury lamp and standard filters for DAPI (UV-2A 360/40; 420/LP), Cy2 (FITC HQ 480/40; 535/50), Cy3 (Cy 3HQ 545/30; 610/75), and Cy5 (Cy 5 HQ 620/60; 700/75). Images were captured using a SPOT Pursuit Digital Camera (Diagnostics Instruments) with the manufacturer's software, and raw TIF files were imported into Adobe Photoshop CS3. Identical adjustments in brightness and contrast were applied to all images in a given experiment.

Corelet activation

Pre-activation and post-activation images of G3BP KO cells stably expressing the indicated fusion proteins were captured with the mCherry (560) channel only to visualize the sspB component without triggering light-induced dimerization with the iLID-mGFP-tagged Ferritin core. Cells were activated with a 488-laser using 1% laser power to cause dimerization of iLID and sspB (Guntas et al., 2015). Activation of cells was achieved by imaging the mCherry and mGFP channels simultaneously using a 6 s frame interval for an area of 120x120 μm^2 (1024x1024 pixels) at Nyquist zoom. See also Phase diagram data collection.

Fluorescence recovery after photobleaching (FRAP)

G3BP KO cells stably expressing indicated fusion proteins were first globally activated to trigger iLID-sspB dimerization by continuously exposing them with the 488 laser for 5-min. Light-activated condensates were then bleached in a ~1 μm^2 region with the 560 laser at high power to quench the majority of the mCherry-sspB component of the condensate. Fluorescence recovery was monitored while imaging both mCherry and mGFP channels at a frame interval of 6 s. Fluorescence was standardized based on a non-bleached droplet in the same cell to control for FRAP-independent bleaching. Fluorescence intensity was compared to the initial image for generating plots.

Cell treatment with arsenite to dissociate polysomes

Cells were "stressed" by adding sodium arsenite (referred to as "As" throughout text) to cell media at a concentration of 400 μM, which is in excess of saturating concentrations for maximal polysome disassembly (Kedersha et al., 2016). Images were captured between 50-min and 2 h (typically 1 h) after arsenite treatment, unless performing activation-deactivation (light-dark) cycling experiments (see below). No differences were observed with respect to rescue of SG defects, phase threshold shift, SG inhibition, etc. between 60- and 120-min. SG number/size typically peaked by 45-min, and 1- to 2 h time window was chosen, so that drug reached maximal effect (i.e., maximum amount of exposed RNA available in the cytoplasm). Cells typically began to die ~6 h following treatment; to avoid confounding toxicity/lethality effects, the indicated 1- to 2 h time window was used.

Inhibition of polysome disassembly by pre-treatment with cycloheximide

Cycloheximide (blocks polysome disassembly) was added to G3BP KO cells expressing indicated fluorescent fusion proteins at a final concentration of 100 μg/mL. Following 30-min of incubation, arsenite was added (400 μM final concentration). 1 h later, cells were assessed for formation of stress granules (GFP-G3BP rescue experiments) or activation cycles were performed (Corelets).

Cell treatment with Actinomycin D to inhibit transcription

Actinomycin D ("ActD"; intercalates into DNA to prevent transcription) dissolved in DMSO was used to treat G3BP KO cells expressing indicated Corelets at a final concentration of 5 μg/mL. Images were taken 12-18 h after Actinomycin D treatment, a time interval

during which nucleoli were no longer visible by bright field microscopy, and the vast majority of mRNA was expected to be degraded. Final concentration of DMSO was 0.5%, which is well below toxic levels. For Actinomycin D plus arsenite experiments, arsenite was added to a final concentration of 400 μM ~12 h following Actinomycin D treatment, and cells were imaged 1-2 h post-arsenite. Qualitative observations suggested that the application of Actinomycin D at the indicated concentration was lethal following ~24-36 h of treatment. The 12 h time point was chosen to maximize the time since treatment (i.e., to reduce RNA in cells by as much as possible) without extensive lethality from the drug.

Phase diagram data collection

In order to determine precise phase threshold boundaries for intracellular phase diagrams, analyzed cells must feature high variability with respect to sspB-mCherry and iLID-mGFP concentrations, so as to sample sufficient core concentrations and valences. In order to achieve a broad concentration range for both components, G3BP KO cells were transduced in 96-well plates using an arrayed lentivirus approach. In this protocol, rows varied from 2 to 60 [2, 6, 20, 60] μL iLID-GFP-Fe lentivirus; columns, 2 to 60 [2, 6, 20, 60] μL mCherry-sspB-protein of interest ("POI") (or POI-mCherry-sspB) lentivirus. G3BP KO cells were plated directly into the arrayed lentivirus to achieve ~25% confluency upon subsequent attachment to the plastic substrate. 72 h later, at confluency, all 16-wells associated with an individual Corelet condition were washed with PBS, trypsinized, quenched with fresh media, and combined into a single test tube, thus ensuring a diverse population of cells with highly variable iLID to sspB ratios. Cells were plated at a 1:8 dilution factor onto fibronectin-coated, glass bottom 96-well plates (Cellvis) and imaged 48 h later when at 60%–90% confluency.

For all data collected toward generation of phase diagrams, a standardized imaging protocol was adopted to avoid confounding effects related to alterations in microscopy settings. Identical imaging settings were used relative to fluorescence correlation spectroscopy (FCS)-based calibrations (fluorescence to absolute concentration) (see Quantification and Statistical Analysis). Specifically, images were collected using 0.5 frames per second scan rate, 1024x1024 pixel frame (120x120 μm^2), and 1.75x Nyquist zoom (63x oil immersion lens). Laser powers (1% 488 and 100% 546), intensities, and gains were kept constant. All time lapses (activation periods) were 5-min in length and featured 6 s intervals between frame acquisitions. Following the last frame, laser intensity was dropped for 4-additional frames followed by acquisition of 4-final images at higher relative laser intensity. This protocol was selected to achieve wide dynamic range (i.e., to achieve sufficient resolution of lower concentration cells, which feature lower signal to noise, and to avoid pixel saturation in cases of exceptionally bright dense phases).

Using this standardized protocol, each 5-min acquisition was able to add (on average) 10-data points (i.e., cells) to a phase diagram. Thus, an average phase diagram reported in this study required collection of 20-30 fields or ~2-3 h of data acquisition time. Typically, an individual phase diagram was compiled from data collected over the course of 3-5 experiments (i.e., different lentivirus transductions on different days). However, certain phase diagrams featured data from significantly more experiments (e.g., G3BP1ΔNTF2 Corelets, a condition used as a positive control for effects of drug treatments throughout studies, which ensured reliability of data). Throughout the duration of the study, there was no indication of systematic changes with respect to drug response, drug efficacy, measurement of fluorescence intensities, or phase diagram threshold shifts.

When selecting cells for analysis, only fully activated cells (entire cell within field of view) were considered to avoid potential artifacts related to local activation and diffusive capture (Bracha et al., 2018). The average mCherry and mGFP fluorescence intensity for a cell was determined using the first frame, prior to blue-light mediated dimerization of iLID on core to sspB-tagged protein of interest, and manual image segmentation of 4.5 × 4.5 μm square regions of interest (ROIs) in cytoplasmic regions featuring homogeneous fluorescence (i.e., regions with low density of membrane-bound organelles like the juxtanuclear Golgi apparatus). The aforementioned FCS calibration curves were then used to determine the mCherry and mGFP concentrations. The mGFP concentration was divided by 24, the number of subunits per ferritin complex or "core," to determine the core concentration. Valence was determined for an individual cell by dividing the mCherry concentration value by that of the core. Previously, we showed that this is a highly accurate measure based on the lever rule—in a "one-component" system (e.g., FUS IDR Corelets, which feature minimal endogenous proteins, nucleic acids; see Figure S2A), consistency in valence between initial, dilute, and condensed phases is reliably observed (Bracha et al., 2018). Binary decisions (yes or no) regarding Corelet-mediated phase separation in a cell of interest were determined manually. Datasets used for subsequent automated generation of phase diagrams and phase thresholds (see QUANTIFICATION AND STATISTICAL ANALYSIS) were coded and sent to a separate individual.

Cycling experiments following drug treatments

Cycling experiments were performed similarly to experiments describes in Phase diagram data collection with minor changes. After treatment of G3BP KO cells expressing indicated sspB/iLID Corelets with arsenite (or indicated drug), image acquisition was immediately commenced. For most experiments, a 5-min activation (488 blue light) time lapse was acquired for each cycle, immediately followed by a 5-min time lapse for deactivation (no 488 blue light). We have determined that this deactivation time far exceeds that which is required for complete reversibility (typically 30-60 s, see Figures 4B; S4A), of diverse Corelet condensates. Indicated cycling parameters were repeated 6-8 times. In certain experiments, instead, a 10-min activation time lapse was immediately followed by a 5-min time lapse for deactivation. This was repeated four times. Intervals were kept constant at 6 s in all cases. Representative cells/fields were chosen for data analysis based on standard core concentrations (~0.25 μM) and desired valence, which is indicated in figure legends for a given experiment.

G3BP rescue competition assay and stress granule inhibition experiments

For G3BP rescue competition experiments (Figure 3), an identical arrayed lentivirus approach was used as described in Phase diagram data collection (i.e., 2-60 μL G3BP1-mCherry and 2-60 μL mGFP-POI, arrayed 4-wells by 4-wells for 16-wells total of a 96-well plate). G3BP KO cells were plated into lentivirus, grown for 72 h, then combined and passaged at 1:8 dilution factor. At the next confluency, cells were passaged to fibronectin-coated 96-well glass plates (Cellvis), and live cell confocal microscopy was performed on Day 8 post-transduction. For each condition (GFP-tagged POI), 4 separate experiments (each experiment = 1-well with arsenite treatment) were performed on three separate days with numerous technical replicates (fields of view or ''images''). Live confocal imaging was performed 1-2 h following arsenite treatment. Concentrations of mCherry and mGFP were determined similarly as for phase diagrams, and manual scoring of stress granule presence or absence was performed. Similar protocols were used to assess stress granule rescue thresholds in the absence of competition.

For stress granule inhibition experiments (Figure S1G; Figure S3B; etc.), WT U2OS cells stably expressing YBX1-mCherry (SG marker protein) were plated into 96-well plates at 25% confluency and transduced with 2-60 μL lentivirus of indicated mGFP-tagged protein (4-wells: 2, 6, 20, or 60 μL). Three days later, cells were washed, trypsinized, combined, and passaged at 1:8 dilution factor. Three days after this, confluent cells were passaged onto fibronectin-coated 96-well plates. Live cell confocal imaging was performed 2-days later (i.e., 8 days following lentivirus transduction) when cells were at 60%–80% confluency. Images were taken between 1-2 h after arsenite treatment. 3-4 independent experiments were performed for each condition on two separate days with numerous technical replicates (i.e., fields of view or ''images'') per experiment. Concentrations of mGFP-tagged proteins were determined using FCS calibration curves, SG formation was assessed in a binary manner, and all data was coded then sent to a separate individual for quantitative analysis.

Stress granule partitioning

For stress granule partitioning experiments, WT U2OS cells stably expressing mGFP-CAPRIN1 (Figure 1I) or mCherry-CAPRIN1 (Figure 6I) were plated into 96-well plates at 25% confluency and transduced with either 30 μL of indicated mCherry-tagged lentivirus (Figure 1I) or mGFP-tagged lentivirus (Figure 6I). Three days later at confluency, cells were washed, trypsinized, and passaged at 1:8 dilution factor. Three days after this, cells were passaged onto fibronectin-coated 96-well glass plates (Cellvis). Live cell confocal imaging was performed 2-days later (i.e., 8 days following lentivirus transduction) when cells were at 60%–80% confluency. Images were taken between 1-2 h after arsenite treatment. Three independent experiments were performed for each condition.

Co-Localization Corelet studies

Followed similar protocol as ''Phase diagram data collection'' but performed two-lentivirus co-transduction (with sspB-mCh-POI and non-fluorescent iLID-Fe instead of typical GFP-tagged version) on G3BP KO cells stably expressing the indicated GFP-tagged protein. 72 h after infection, cells were passaged at 1:8 dilution factor onto fibronectin-coated, glass bottom 96-well plates (Cellvis). 48 h later, cells were treated with arsenite (400 μM). One h later, removed plate from humidified incubator and placed on a blue LED light illuminator (Invitrogen SafeImager 2.0) for 10-min to activate Corelets. Immediately fixed with 4-percent PFA for 10 min. Washed twice with PBS and permeabilized with ice cold 70% methanol for 10 min. Washed an additional two times with PBS then placed at 4°C overnight. Performed fixed cell confocal microscopy the next day to examine co-localization of opto-SGs with indicated GFP-tagged proteins. Multiple replicates (images) were taken and representative examples are shown.

RNA fluorescence *in situ* histochemistry (RNA-FISH)

Indicated cells were fixed with 4-percent PFA for 10-min then washed twice with PBS and permeabilized with ice cold 70% ethanol. 96-well glass bottom plates (Cellvis) were placed at −4°C overnight. The next day, ethanol was replaced with Wash Buffer A (Stellaris) and incubated at room temperature for 5-min. Buffer A was then replaced with hybridization buffer (Stellaris) containing 5 μM 5′-Cy5-Oligo d(T)20 (Gene Link) (hybridizes to polyA tails of mRNA) and incubated in the dark for 16 h to probe polyadenylated mRNA. Hybridization buffer was replaced with Wash Buffer A, placed at 37°C for 30-min, then replaced with Wash Buffer B, incubating at room temperature for another 5-min. Following three PBS washes, cells were imaged with Nikon A1 laser-scanning confocal microscope.

Western blot to assess G3BP1/2 levels and knockout

For Figure S1B, confluent human cell lines (U2OS WT, U2OS G3BP1/2 KO, HEK293, HeLa) from a 6-well plate were washed, trypsinized, quenched with media, harvested, and centrifuged at 500xg for 5-min. Cell pellets were washed with PBS and flash-frozen. Immediately prior to lysis, cells were thawed on ice and re-suspended in 150 μL 2x Nuage® LDS Sample Buffer/Reducing agent, sonicated, and boiled at 100°C for 5-min. 50 ng of the following recombinant proteins were loaded in lanes alongside cell lysates as positive controls: G3BP1 (Novus, NBP1-50925-50UG), G3BP2 (Novus, NBP1-78843-100UG). Samples were run on a NuPAGE® Novex 10% Bis-Tris Gel and transferred to PVDF Pre-Cut Blotting Membranes, as per manufacturer's protocol. Membranes were blocked overnight at 4°C with rocking in 5% NFDM in TBST (5 mM Tris-HCl, pH 7.5, 15 mM NaCl, 1% Tween-20). Membranes were probed with the following primary antibodies in blocking solution overnight at 4°C with rocking: G3BP1 (Mouse monoclonal, AbCam ab86135, 1:300), G3BP2 (Rabbit polyclonal, AbCam ab86135, 1:5000), Beta actin (Rabbit polyclonal, AbCam ab8227, 1:10,000). The next day, membranes were washed multiple times and then incubated with the following secondary antibodies in blocking solution for 30-min at room temperature with rocking: Peroxidase-AffiniPure Goat Anti-Mouse IgG (H+L) (Jackson, 115-

035-062, 1:10,000), Peroxidase-AffiniPure Goat Anti-Rabbit IgG (H+L) (Jackson, 115-035-144, 1:10,000). Subsequently, multiple washes were performed prior to developing the membrane using SuperSignal West Pico PLUS Chemiluminescent Substrate, as per manufacturer's instructions.

Immunoprecipitation of high-affinity protein complexes from U2OS Cells

150 mm dishes of near-confluent cells were treated as indicated, washed with cold Hanks Basic Salt Solution, and scrape-harvested at 4°C into lysis buffer (20 mM Tris-HCl pH 7.4, 150 mM NaCl, 5 mM MgCl2, 1 mM DTT 0.5% NP-40, 10% glycerol) containing 1 mM DTT, protease inhibitors (Roche, EDTA free), HALT phosphatase inhibitors (Pierce), and 20 μg/nL RNase A. Cells were rotated for 30-min at 4°C, cleared by centrifugation (5000 rpm for 5-min), and supernatants removed then incubated with Chromotek-GFP-Trap® Beads (Allele Biotech) for 2 h with continuous rotation at 4°C. Beads were washed 5-times, and either eluted directly into SDS-lysis buffer with RNase treatment, or extracted in RIPA buffer (50 mM TRIS, 150 mM NaCl, 1.0% NP40, 0.5% DOC, 0.05% SDS) for 1 h at 4°C with rotation. Material released by RIPA buffer was recovered and precipitated with 60% acetone. Beads post-RIPA extraction contained bound material denoted "high-affinity," which was released by heating in reducing SDS-PAGE lysis buffer. Proteins were resolved on 4%–20% Mini-PROTEAN TGX Precast Gel (Bio-Rad), transferred to nitrocellulose membranes using the Transfer-Blot Turbo transfer system (Bio-Rad), and blotted using standard procedures as above. Chemiluminescence was detected using Super-Signal West Pico substrate (Thermo Scientific).

CRISPR-Cas9 generation of KO cell lines and validation

Please see Table S2 for information regarding generation of U2OS knockout cell lines. Each target sequence (see table) was purchased as paired DNA oligos (sense/anti-sense pairs) from IDT, annealed, and ligated into pCas-Guide (Origene), with the exception of UBAP2 (see below). Plasmid inserts were verified by sequencing, and transfected into cells with pDonor-D09 (Origene, encodes puromycin resistance). Following transfection, cells were subjected to a brief (24 h) selection in puromycin (2 μg/mL) and allowed to recover for 2-days or longer before evaluation using the indicated antibodies and immunofluorescence. Cells were cloned by limiting dilution, and clones were verified using both immunostaining and western blotting.

For single KO lines, the parental cell line was U2OS expressing the Tet-repressor (Kedersha et al., 2016). CAPRIN1 and USP10 were individually knocked out in the previously characterized G3BP1 and G3BP2 double KO (G3BP1/2 or G3BP KO) cells (Kedersha et al., 2016). To create the U2OSΔFXR1/FXR2/FMR1 (3KO) cell line, FXR2 was first KOed, clones were selected, and FXR2 protein expression was evaluated by immunofluorescence and western blotting. "Clone 6" was then transfected with guide RNAs targeting *FXR1* and *FMR1*. Clones were selected and screened in a similar manner and finally a triple null line (3KO) was obtained. All loci were sequenced to confirm deletions in the DNA.

In the case of UBAP2/UBAP2L double KO (2KO), validated UBAP2L single-KO cells were plated into 200 μL of pCRISPRv2-UBAP2 gRNA (pooled, 6 gRNAs) or 200 μL of pCRISPRv2-NonTarget gRNA (Shalem et al., 2014) in 96-well plate. 72 h later, confluent cells were washed, trypsinized and passaged into new wells containing 200 μL of the same lentivirus. Cells were passaged three times and examined for successful KO by immunofluorescence, validating with two antibodies against UBAP2, which indicated that ~30 percent of the cells featured very low or undetectable levels of UBAP2 (in NonTarget control, 100% of cells displayed UBAP2 staining). Cells were amplified by three successive 1:8 passages in 96-well plates over a 1-week period. Upon the third confluency in 96-well, cells were passaged at limiting dilution into three separate 96-well plates, so that each well featured ~50% chance of receiving a cell. 10 days later, colonies were apparent in ~20%–30% of wells. For NonTarget control, six wells were harvested and passaged; candidate UBAP2 and UBAP2L double-KOs (UBAP2/2L 2KO), 50 separate lines. Following approximately two weeks of additional passage and growth, candidate KO lines (and NonTarget controls) were plated onto fibronectin-covered glass (96-well plate). 24 h later, cells were at ~60%–80% confluency. Cells were fixed with 4% PFA, permeabilized with ice-cold methanol for 5-min, and immunofluorescence was performed (anti-UBAP2, anti-G3BP1). In NonTarget controls (i.e., UBAP2L 1KO), most cells featured G3BP-positive stress granules but they were slightly smaller than control conditions (i.e., WT cells), a result that was validated across labs (data not shown). Four candidate UBAP2/2L double KO lines featured undetectable UBAP2 by immunofluorescence. In these examples, G3BP-positive SGs were only present in ~30% of cells and they were much smaller in size than in WT or UBAP2L single-KOs. Double knockout of UBAP2 and UBAP2L was confirmed in three lines and relative levels of G3BP1, G3BP2, USP10, and CAPRIN1 were assessed by western blot.

Genotyping of Cas9 mutant cell lines

To identify Cas9-induced mutations of all KO cell lines in the coding sequence, genomic amplification was performed using nested primer sets surrounding the region targeted by the particular guide sequence. Genomic DNA PCR was done with Invitrogen's AccuPrime GC-Rich DNA Polymerase (Buffer A). DNA was initially denatured at 95°C for 3-min, followed by denaturation at 95°C for 30 s, annealing at 60°C for 30 s, and extension at 72°C for 1-min for 30 cycles. Final extension was done at 72°C for 10-min. PCR amplicons were directly sequenced. If there was evidence for multiple sequences (i.e., multiple alleles), PCR products were adenylated using Taq polymerase and cloned into Promega pGEM®-T Easy vector; individual clones were obtained and sequenced.

Double-positive U2OS stable cell lines

A clonal cell line was made constitutively expressing mCherry-G3BP1 by transfection of mCherry-G3BP1-C1 into the G3BP1/2 (G3BP) KO cells containing the Tet repressor, selected using G418 (500 μg/mL), and cloned. This line was used to make double-positive cells expressing Tet-inducible GFP-tagged proteins (G3BP1 WT, G3BP1 S38F, G3BP1 F33W, and UBAP2L WT) in pcDNA4 t/o vector (Invitrogen), selected using zeocin (Invitrogen, 250 μg/mL). These cell lines were used for immunoprecipitation experiments in Figure 2 and Figure 6.

QUANTIFICATION AND STATISTICAL ANALYSIS

Fluorescence correlation spectroscopy

GFP and mCherry fluorescence values were converted to absolute concentrations using fluorescence correlation spectroscopy (FCS), performed as described previously (Bracha et al., 2018) with minor modifications. Data for diffusion and concentration of indicated fluorescent fusion proteins were obtained with 30 s FCS measurement time. The measurements were performed on U2OS G3BP1/2 2KO ("G3BP KO") cell populations expressing iLID-mGFP or mCherry-sspB, fusion protein conditions that were chosen based on the assumption that such non-native fusion proteins would be monomeric and feature no major endogenous binding partners. Images were taken using a Nikon A1 laser scanning confocal microscope with an oil immersion objective (Plan Apo 60X/1.4 numerical aperture, Nikon). All measurements and data analysis were performed using the SymPhoTime Software (PicoQuant). The autocorrelation function for simple diffusion is:

$$G(\tau) = G(0)\left(1+\left(\frac{\tau}{\tau_D}\right)\right)^{-1}\left(1+\left(\frac{\tau}{\kappa^2\tau_D}\right)\right)^{-0.5}$$

The variables in the above equation are defined as follows: $G(0)$ is magnitude at short timescales; τ is the lag time; τ_D is the half decay time; and κ is the ratio of axial to radial of measurement volume ($\kappa = (\omega_z/\omega_{xy})$. Here, ω_{xy} = 0.19 μm and κ = 5.1, which is determined by the fluorophore dye Alexa488 in water. The parameters τ_D and $G(0)$ are optimized in the fit and are used to determine the diffusion coefficient ($D = \omega_{xy}^2/4\tau_D$) and molecule concentration ($C = (\pi^{\frac{3}{2}}\omega_{xy}^2\omega_z G(0))^{-1}$).

The fluorescence to concentration calibration curves displayed in Figure S1C were used for all experiments that quantitatively assess the concentrations of mCherry- and mGFP-tagged fusion proteins in WT and G3BP KO U2OS cells. Such FCS calibration curves yielded several findings that support the precision of such estimates. These are detailed below.

First, independently performed mCherry FCS experiments yielded concentration estimates that were < 5% different from previous measurements (Bracha et al., 2018). Further, the aforementioned study used an autocatalytic P2A system to co-express mGFP and mCherry at equimolar ratios, with GFP concentrations extrapolated from the FCS calibration curves determined for mCherry. This indirectly extrapolated calibration curve predicted GFP concentrations that differed by < 20% from the independently obtained calibrations and estimations used in this study.

Second, the slope determined in Figure 3B, which quantifies stoichiometry between USP10 and G3BP required to differentiate cells that form stress granules from those that are unable to, is remarkably close to 1 (~0.98). A slope of 1 is predicted for such a competitive inhibitor ("cap") expressed at concentrations far greater than its K_d and is further confirmed by nearly equivalent slopes for other strong inhibitors ("caps" e.g., USP10 NIM and CAPRIN1 NIM).

Third, we estimated the concentration of G3BP1/2 in U2OS cell cytoplasm by adding the G3BP concentration for rescue (620 nM) (Figure 3B) and USP10 concentration for SG inhibition (1560 nM) (Figure S3B) to extrapolate a concentration of ~2180 nM. This value is approximately equal to independently obtained mass spectrometry values in HeLa cells (1808 nM in cytoplasm, a value extrapolated from the reported estimate of 1446 nM in whole cells, based on the assumption that the nucleus accounts for 20% of total volume and all G3BP is located to the cytosol (Hein et al., 2015)). Importantly, western blot confirms similar levels of both G3BP1 and G3BP2 in HeLa and U2OS cells (Figure S1B).

Fourth, we determined that mGFP-G3BP1 and G3BP1-mCherry feature identical SG rescue concentration thresholds (Figure S1D, within 50 nM of each other), despite different fluorescent protein tags. Taken together, these observations give confidence that our FCS calibration curves are highly accurate for estimating fluorescent protein concentration in living cells.

Image analysis

All images were analyzed using a combination of manual image segmentation (ImageJ), custom semi-automated workflows in ImageJ, and automated analysis in MATLAB 2018b. In all experiments, regions of interest were selected in ImageJ and average cytoplasmic intensities were calculated using the aforementioned FCS calibration curves. The presence of stress granules was, in cases other than the cycling experiments, determined by manual scoring based upon co-localization with a protein marker of stress granules that features diffuse distribution in the cytoplasm in the absence of stress (and further, is diffuse in the cytoplasm of stressed G3BP KO cells without ectopic expression of a protein that rescues stress granule defects).

Manual image segmentation

The average fluorescence intensity for mCherry and mGFP in an individual cell was used to approximate the concentration of associated fusion proteins. This was determined by using manual image segmentation (ImageJ) to draw 4.5 × 4.5 μm square ROIs in cytoplasmic regions featuring homogeneous distribution of fluorescence (i.e., regions with low density of membrane-bound organelles like the Golgi). The aforementioned FCS calibration curves were then used to determine the protein's concentration. Presence or absence of stress granules was manually annotated. For Corelet phase diagrams, phase separation was assessed based on whether visible ''puncta'' formed following a 5-min activation time course (6 s intervals between images). Only fully activated cells were considered to avoid confounding effects related to diffusion-based capture (Bracha et al., 2018).

Light-dark cycling experiments

Individual regions of interest, which remained in the field of view throughout the time course, were manually selected. Standard deviations were calculated from the measured mCherry intensity and were normalized by the standard deviation at the first frame taken.

G3BP rescue competition data analysis in G3BP KO U2OS cells

The concentration of each cell was determined via manual image segmentation as previously described, and absence or presence of stress granules was annotated. To determine a boundary from the data, a support vector machine (SVM) trained using the concentrations of the two components as explanatory variables and the categorical stress granule state as a response variable by applying the *fitcsvm()* function in the MATLAB Statistics and Machine Learning package using the default solver. Briefly, a support vector machine constructs a linear decision surface based on boundary points (''support vectors''), with the assumption that the data is linearly separable. In this two-dimensional case, the parameters of slope and intercept were extracted to calculate the minimal G3BP concentration for stress granule formation as well as the stoichiometry of interactions with proteins of interest (i.e., the slope of the corresponding line).

Phase diagrams and calculation of threshold valence

For each phase diagram, mean concentrations of both iLID-GFP-Fe core and mCherry-sspB-tagged proteins were calculated and assigned to the category of having or not having stress granules. To determine phase threshold boundaries in an automated and unbiased fashion, an SVM regressor was again used, using the core concentration and log2-transformed valence as explanatory variables with the presence of phase separated structures as a categorical response variable. However, because the data was not linearly separable, a polynomial kernel with degree = 2 was used to account for the curvature of the phase threshold. Then, to calculate the decision surface, the score of the SVM was calculated at all points in a 50-by-50 grid in the phase diagram, and a contour line representing the phase threshold was drawn connecting points with a score of 0 using MATLAB's *contour*() function. Specific values for threshold valence at specified core concentrations were then calculated by linearly interpolating the zero-score contour line.

Quantification of threshold concentration for inhibition of stress granule assembly (WT cells) or rescue (G3BP KO cells)

For each experiment, the concentration of the protein of interest was determined for each cell, and the presence (or absence) of stress granules was categorized. The threshold concentration of inhibition (or rescue) was defined as the concentration of protein of interest at which cells had a 50 percent chance of having stress granules. Specifically, the probability density was calculated by binning the concentration distribution using a square root number rule. Within each bin, the probability of having stress granules was calculated as the number of cells with stress granules over the total number of cells in that bin. This results in a monotonic function; its value at a probability of 0.5 was then interpolated to determine the threshold concentration of inhibition or rescue. This was repeated for each replicate and standard error of the mean between replicates was used to determine error bars. The bin size was used as the error if it was greater than that calculated for the SEM or in experiments with a single replicate.

Partitioning coefficient image analysis

To determine partition coefficients (PCs) of fluorescently tagged proteins of interest into stress granules (marker = GFP-CAPRIN1 or mCherry-CAPRIN1), confocal microscopy images were taken at three different settings to prevent oversaturation of the images in both fluorescent channels (488, GFP; 546, mCherry). For each set of images, the image with the highest intensities yet lacking saturated pixels was analyzed. Stress granules (SGs) were first segmented in the CAPRIN1 channel by applying a Laplacian of Gaussians (LoG) filter with a kernel size of 6-pixels to the image. The resulting image was then thresholded and a mask from pixels with a LoG intensity of greater than 1.5 standard deviations was generated. Pixels near the border of the image or SGs containing fewer than 9-pixels were removed from the analysis. To determine the intensity inside SGs while avoiding intensity gradients near the edge of the SGs, masks were thinned. Likewise, to calculate the background intensity near but outside the SGs, an annulus was constructed by subtracting a mask thickened 8-times from that thickened 4-times from the original thresholded image (bwmorph, MATLAB2018b). Then, for each identified SG, an average intensity inside and outside the SG was calculated by background subtracting and averaging the intensities of the corresponding pixels in the fluorescently tagged protein of interest channel based on the aforementioned segmentation of the CAPRIN1 channel. The partition coefficient (PC) was calculated by solving the following

linear system: PC*I_{in} = I_{out} (mldivide, MATLAB2018b). Error was calculated from the standard error of the mean of intensity I_{in} and I_{out} and then propagated by combining in quadrature.

Model of PPI network phase separation

We adapted the SAFT formalism (Chapman et al., 1989) to model a mixture of colloidal particles with associative interactions, in which each binding site can engage in at most one bond at a time. A colloid in this model refers either to a protein monomer or complex, or to a substrate monomer. Denoting the number of binding sites of type A on a colloid of type i by f_{iA}, we used a prescribed PPI network to specify which binding site pairs (iA, jB) are allowed to interact. Our SAFT-based approach requires two key approximations (Jacobs et al., 2014): First, we used a mixture of colloids with no attractive interactions as the reference state, which means that spatial correlations due to associative interactions are not taken into account. Second, the functional form of the free energy assumes that correlations among binding site availabilities can be ignored.

Defining the volume fraction occupied by colloids of type i as ϕ_i, the total dimensionless Helmholtz free energy density, F/kT, is (Jacobs et al., 2014; Michelsen and Hendriks, 2001)

$$\frac{F}{kT} = \frac{F_{\text{ref}}}{kT} + \sum_i \left(\frac{\mu_{\text{assoc},i}}{kT}\right)\phi_i - \frac{P_{\text{assoc}}}{kT},$$

$$\frac{F_{\text{ref}}}{kT} = \sum_i \phi_i \log \phi_i + \left(1 - \sum_j \phi_j\right) \log\left(1 - \sum_j \phi_j\right),$$

$$\frac{\mu_{\text{assoc},i}}{kT} = \sum_A f_{iA} \log X_{iA},$$

$$\frac{P_{\text{assoc}}}{kT} = -\frac{1}{2}\sum_i \phi_i \sum_A f_{iA}(1 - X_{iA}),$$

where F_{ref} is the free energy of a reference system of colloids with no attractive interactions; $\mu_{\text{assoc},i}$ and P_{assoc} are the associative contributions to the chemical potential of colloid type i and the pressure, respectively; and X_{iA} denotes the fraction of binding sites of type A on a colloid of type i that are unbound at equilibrium. The expression for X_{iA} is given by the chemical equilibrium equations

$$X_{iA} = \left[1 + \sum_j \phi_j \sum_B f_{jB} X_{jB} \Delta_{iA,jB}\right]^{-1},$$

which must be solved self-consistently at fixed $\{\phi_i\}$. The interaction parameters $\{\Delta_{iA,jB}\}$ are non-zero only for binding site pairs that are connected in the prescribed PPI network. We choose to work in the strong-binding regime, taking $\Delta_{iA,jB} = 10^4$ for all interacting binding site pairs, so that X_{iA} is determined primarily by the topology of the PPI network.

Phase coexistence and free-energy landscape calculations

We identified the conditions for phase coexistence in two steps. First, we calculated the convex hull of a grid of points $(\{\phi_i\}, F[\{\phi_i\}]/kT)$ (Mao et al., 2019; Wolff et al., 2011). We identified facets of the hull that correspond to coexistence regions by comparing the distances between the vertices of the facets to the minimum distance between adjacent points on the grid. In this way, we concluded that at most three phases can simultaneously coexist given the networks in Figures 7A and 7B, and that at most two phases can coexist given the networks in Figures 7C and 7D. The values of $\{\phi_i\}$ at the vertices of a facet approximate the coexistence concentrations at the chemical potential vector, $\{\mu_i/kT \equiv \partial(F/kT)/\partial\phi_i\}$, determined from the facet normal vector.

We then used the discretized convex hull results as a starting point for higher-precision phase-coexistence calculations. These off-grid calculations were used to tune $\{\phi_i\}$ and $\{\mu_i\}$ to ensure equal chemical potentials and pressures among all phases, as required for coexistence at equilibrium (Rubinstein, 2003). However, specifying three-phase (two-phase) coexistence in a mixture of four colloid types leaves two (three) other degrees of freedom undetermined. We therefore needed to specify the chemical potential differences among three components in Figures 7A and 7B and among four components in Figures 7C and 7D. In Figure 7A, we started from the coexistence facet with $\{\mu_i\}$ closest in chemical potential space to the centroid of all three-phase coexistence facets, and then fixed the chemical potential differences $\mu_{\text{Node1}} - \mu_{\text{Substrate}} = 0.85kT$ and $\mu_{\text{Bridge}} - \mu_{\text{Node1}} = 3.5kT$. For the sake of comparison, we chose the same fixed chemical potential differences in Figures 7B–7D. In Figures 7C and 7D, we chose the additional chemical potential difference $\mu_{\text{Node2}} - \mu_{\text{Bridge}}$ to be equal to the value obtained from the three-phase coexistence calculation in Figure 7A.

To generate the free-energy plots shown in Figure 7, we calculated

$$\frac{\Delta F\left(\{\phi_i\},\left\{\mu_i^{(\mathrm{coex})}\right\}\right)}{kT}=\frac{F(\{\phi_i\})}{kT}-\sum_i\left(\frac{\mu_i^{(\mathrm{coex})}}{kT}\right)\phi_i,$$

at the coexistence chemical potential vector $\{\mu_i^{(\mathrm{coex})}\}$. We then plotted $\Delta F/kT$ along a linear path through concentration space, $\{\Delta\phi_i\}$, between each pair of coexisting phases. In Figures 7C and 7D, where there is no stable α phase, we calculated the free energy along a linear path to the location of the α phase in panel A. The compositions reported on the free-energy plots are the volume fractions of the components present in each phase, normalized by the total colloid volume fraction in that phase and rounded to the nearest 5%.

We note in the main text that the increased free-energy barrier height between the α and β phases in Figure 7B tends to disfavor wetting of these phases. Strictly speaking, the three-phase junction (α, β, and dilute) pictured in the cartoon in Figure 7A is mechanically stable when the surface tension between the α and β phases, $\gamma_{\alpha\beta}$, is less than the sum of the surface tensions between the other pairs of phases, $\gamma_{\alpha\mathrm{Dil}}+\gamma_{\beta\mathrm{Dil}}$ (de Gennes, 2004). According to the Cahn–Hilliard theory of planar interfaces (Cahn and Hilliard, 1958),

$$\gamma_{\alpha\beta}\propto\int_\alpha^\beta d\left(\Delta\phi_{\alpha\beta}\right)\left[\Delta F\left(\Delta\phi_{\alpha\beta}\right)/kT\right]^{1/2}$$

where $\Delta\phi_{\alpha\beta}$ is the distance along a linear path in concentration space between the phases α and β. Assuming that the constant of proportionality is roughly the same for all pairs of phases, we find that $\gamma_{\alpha\beta}\lesssim\gamma_{\alpha\mathrm{Dil}}+\gamma_{\beta\mathrm{Dil}}$ in Figure 7A, while $\gamma_{\alpha\beta}>\gamma_{\alpha\mathrm{Dil}}+\gamma_{\beta\mathrm{Dil}}$ in Figure 7B. Nevertheless, the true morphologies depend on the exact values of these proportionality constants, the minimum-free-energy paths through concentration space that connect the phases, the curvature of the physical interfaces, and other details that are beyond the scope of this minimal model.

Importantly, the qualitative features of these plots, including the number of phases in the coexistence region and the relative heights of the barriers, are relatively insensitive to the choice of $\Delta\mu$ values. We also verified that these qualitative features are not sensitive to variations in the relative binding interaction parameters.

DATA AND CODE AVAILABILITY

The raw imaging datasets and associated custom MATLAB code supporting the current study have not been deposited in a public repository because of their large size (~1 TB) but are available from the corresponding author on request.

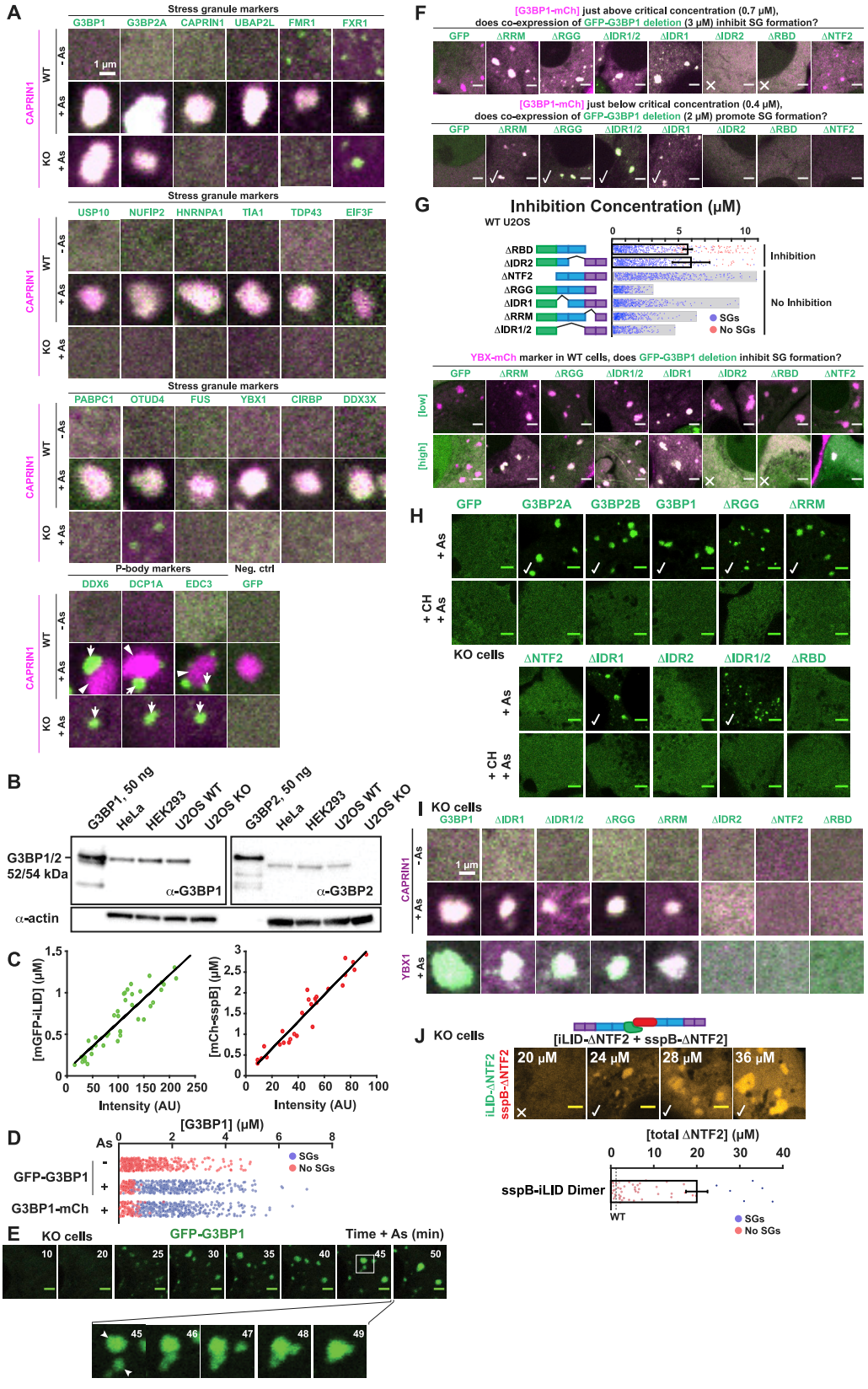

(legend on next page)

Figure S1. G3BP Dimerization and RNA Binding Are Necessary but Not Sufficient for Stress Granule Formation, Related to Figure 1

(A) Wild-type (WT) and G3BP1/2 KO ("G3BP KO") U2OS cells expressing mCherry (mCh)-CAPRIN1 (SG protein) with indicated GFP-tagged proteins (+/− 400 μM arsenite, "As"; 1 h). Lentivirus-mediated stable expression used in all experiments unless specified. Indicated: arrows, P-bodies (PBs); arrowheads, stress granules (SGs).

(B) Western blot of lysate from indicated cells (antibody, α; actin = loading control). 50 ng of recombinant G3BP1 or G3BP2 used as controls.

(C) Fluorescence correlation spectroscopy (FCS) calibration curves to approximate GFP and mCh concentrations in U2OS cells. iLID-GFP and mCh-sspB were used for calibrations due to lack of binding partners, predicted monomeric state, and common use as tags in studies.

(D) G3BP KO cells expressing G3BP1-mCh or GFP-G3BP1 assayed for SG formation (+/−As). Each dot = separate cell (red, no SGs; blue, SGs). Data pooled from n = 4 experiments, >4 images per.

(E) G3BP KO cells expressing GFP-G3BP1 were As-treated. Inset shows fusion of SGs (arrowheads) and relaxation to a sphere. Scale bar, 3 μm.

(F) G3BP KO cells (+As) expressing G3BP1-mCh and indicated GFP-tagged G3BP1 domain deletion were scored for SGs to assess whether deletions inhibit (top, X) or promote (bottom, check) rescue. Scale bar, 3 μm.

(G) WT U2OS cells expressing YBX1-mCh (SG protein) and indicated GFP-G3BP domain deletion were As-treated and SGs were scored. Each dot = separate cell. Mean and SEM: 3-4 experiments, >4 images per. Representative images (X, inhibition). Scale bar, 3 μm.

(H) G3BP KO cells were pretreated with cycloheximide (CH, 30-min, blocks polysome disassembly) followed by As (1 h) and compared to cells that did not receive CH. Checks indicate SGs. Scale bar, 3 μm.

(I) Representative images of G3BP KO cells expressing mCh-CAPRIN1 or YBX1-mCh with indicated GFP-tagged G3BP domain deletion (+/− As).

(J) G3BP KO cells were transfected (Lipofectamine) with iLID-GFP-G3BP1ΔNTF2 and sspB-mCh-G3BP1ΔNTF2 (synthetic RBD dimer). 18 h later, cells were As-treated (1 h), and SGs assessed. Mean and SEM: n = 3 experiments, 4 images per. Dashed line: SG rescue threshold for full-length G3BP1 ("WT"). Top: Representative images (X, no SGs; check, SGs). Scale bar, 3 μm.

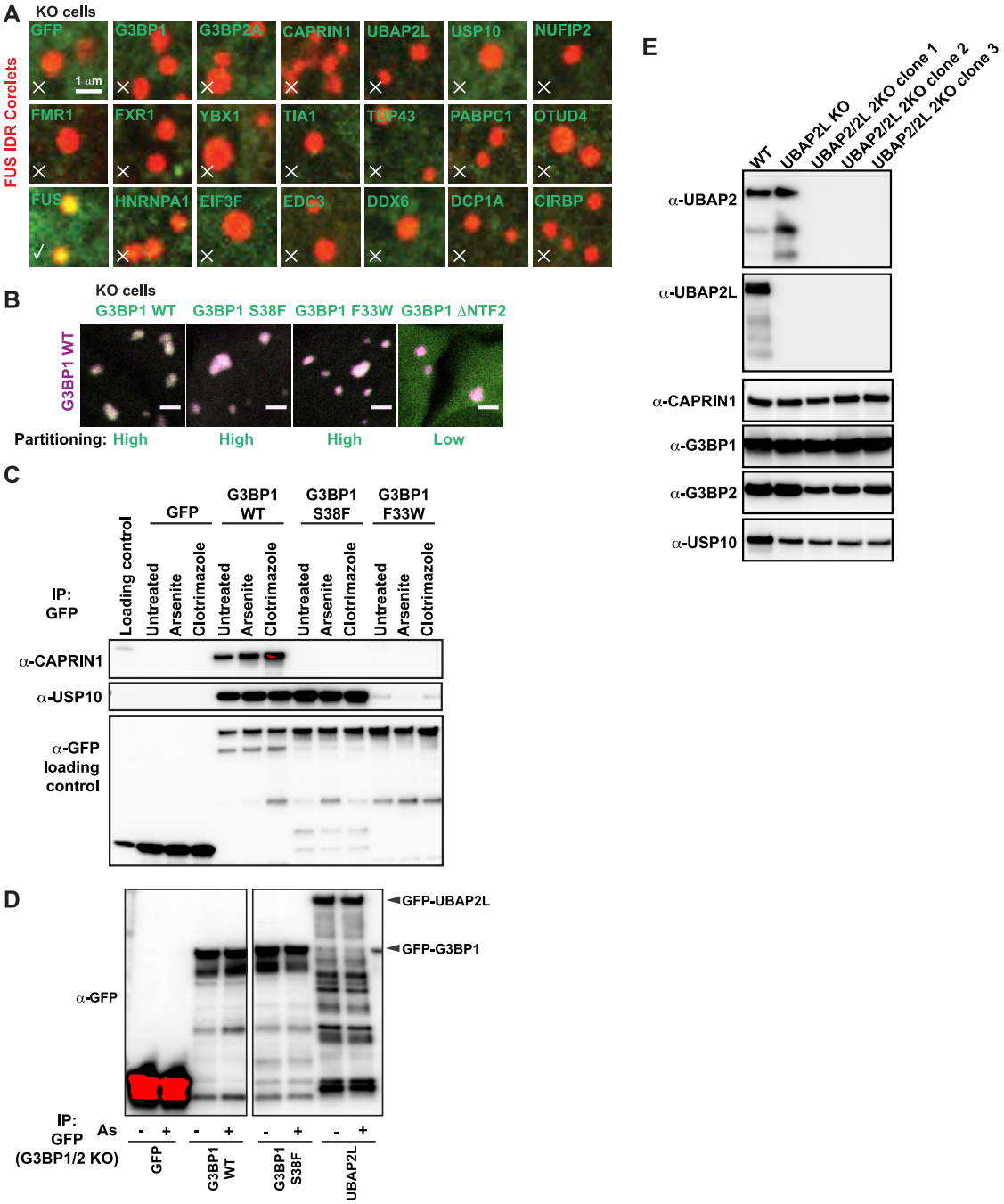

Figure S2. Stress Granule Condensation Requires G3BP-UBAP2L Complexes, Related to Figure 2

(A) G3BP KO cells expressing FUS IDR Corelets (iLID-Fe core, non-fluorescent; FUS IDR-sspB-mCh, red) and indicated GFP-tagged protein were activated (10-min) and fixed. Representative images: check, recruited; X, not recruited.

(B) G3BP KO cells expressing mCh-G3BP1 and indicated GFP-tagged G3BP1 variant were As-treated (1 h). Representative images: scale bar, 3 μm. Relative SG partitioning indicated.

(C) Indicated GFP-tagged proteins were immunoprecipitated ("IP") from G3BP KO cells (treated with indicated drug) with α-GFP followed by RNase and RIPA-wash to isolate tightly bound proteins (assessed with antibody α).

(D) Loading control for Figure 2D: IP of indicated GFP-tagged protein expressed in G3BP KO cells (+/− As).

(E) Western blot of WT, UBAP2L 1KO, and UBAP2L 2KO U2OS cell lines (three separate clones) to assess expression levels of indicated proteins.

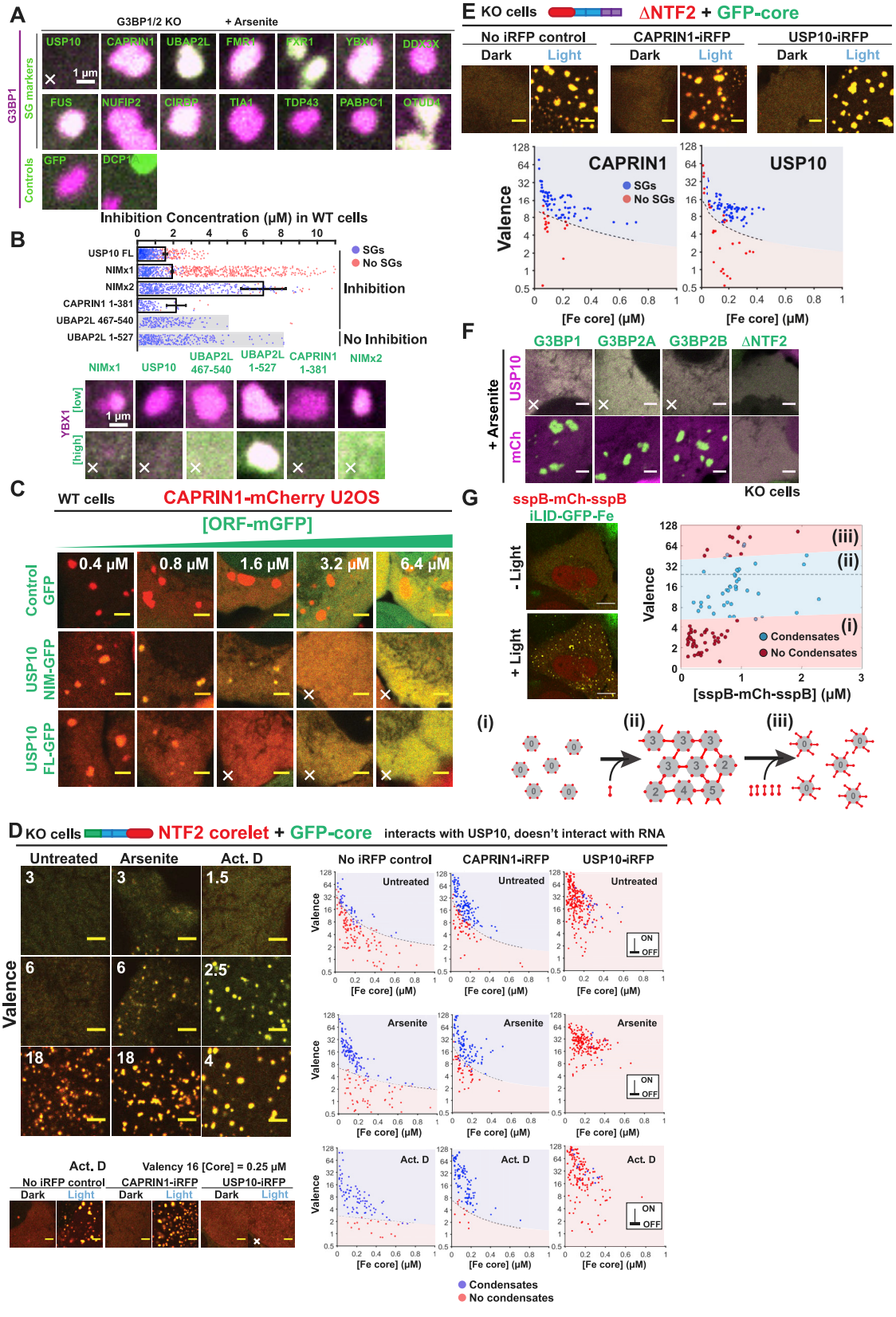

(legend on next page)

Figure S3. Valence Capping of the G3BP Node by RBD-Lacking Binding Partners Prevents Stress Granule Formation, Related to Figure 3

(A) As-treated G3BP KO cells expressing mCh-G3BP1 (~1 μM) and indicated GFP-tagged protein (~2-4 μM). X = inhibits SGs.

(B) WT U2OS cells expressing YBX1-mCh (SG protein) and indicated GFP-tagged protein were As-treated and SG formation was assessed (each dot, separate cell). Mean and SEM: n = 3 experiments, >4 images per. Representative images (bottom): X = SG inhibition.

(C) WT U2OS cells expressing CAPRIN1-mCh (SG protein) and indicated GFP-tagged protein. GFP concentrations are noted at top of column. X = inhibits SG formation. Scale bar, 3 μm.

(D) G3BP KO cells expressing indicated iRFP-tagged protein and G3BP1ΔRBD ("NTF2") Corelets were treated with drug (ActD, 12 h; As, 1 h), activated (5-min), and examined for LLPS. Top left: Representative images for cells with core~0.25 μM and indicated valence (*v*). All images: scale bar, 3 μm. Bottom left: ActD-treated cells expressing indicated iRFP-tagged protein and NTF2 Corelets (core~0.25 μM, *v*~16): X = inhibition of LLPS. Right: Intracellular phase diagrams for NTF2 Corelets expressed with iRFP-tagged proteins in G3BP KO cells (drug treatment shown). Each dot = single cell. Calculated best-fit phase threshold.

(E) G3BP KO cells expressing indicated iRFP-tagged protein and G3BP1ΔNTF2 Corelets were As-treated, activated (5-min), and examined for LLPS. Top: Representative images at core~0.25 μM and *v*~8. Scale bar, 3 μm. Bottom: calculated best-fit phase threshold. Compare to Figure 4F.

(F) G3BP KO cells expressing indicated mCh-tagged protein and GFP-tagged G3BP isoform/deletion were As-treated and scored for SGs (X = inhibition by mCh-tagged protein). Scale bar, 3 μm.

(G) G3BP KO cells expressing sspB-mCh-sspB cross-linker Corelets were activated (5-min) and examined for LLPS. Left: Representative images at sspB~1 μM, *v*~16. Scale bar, 3 μm. Right: Qualitative phase thresholds show reentrant phase transition (blue, LLPS; red, no LLPS). Bottom: Patchy colloid-inspired schematic describing re-entrant LLPS. At low sspB concentrations (left), average core *v* is insufficient to form space-spanning network, unlike medium concentrations (middle). At high concentrations (right), binding sites on cores are saturated, cross-links cannot occur, and network formation is inhibited.

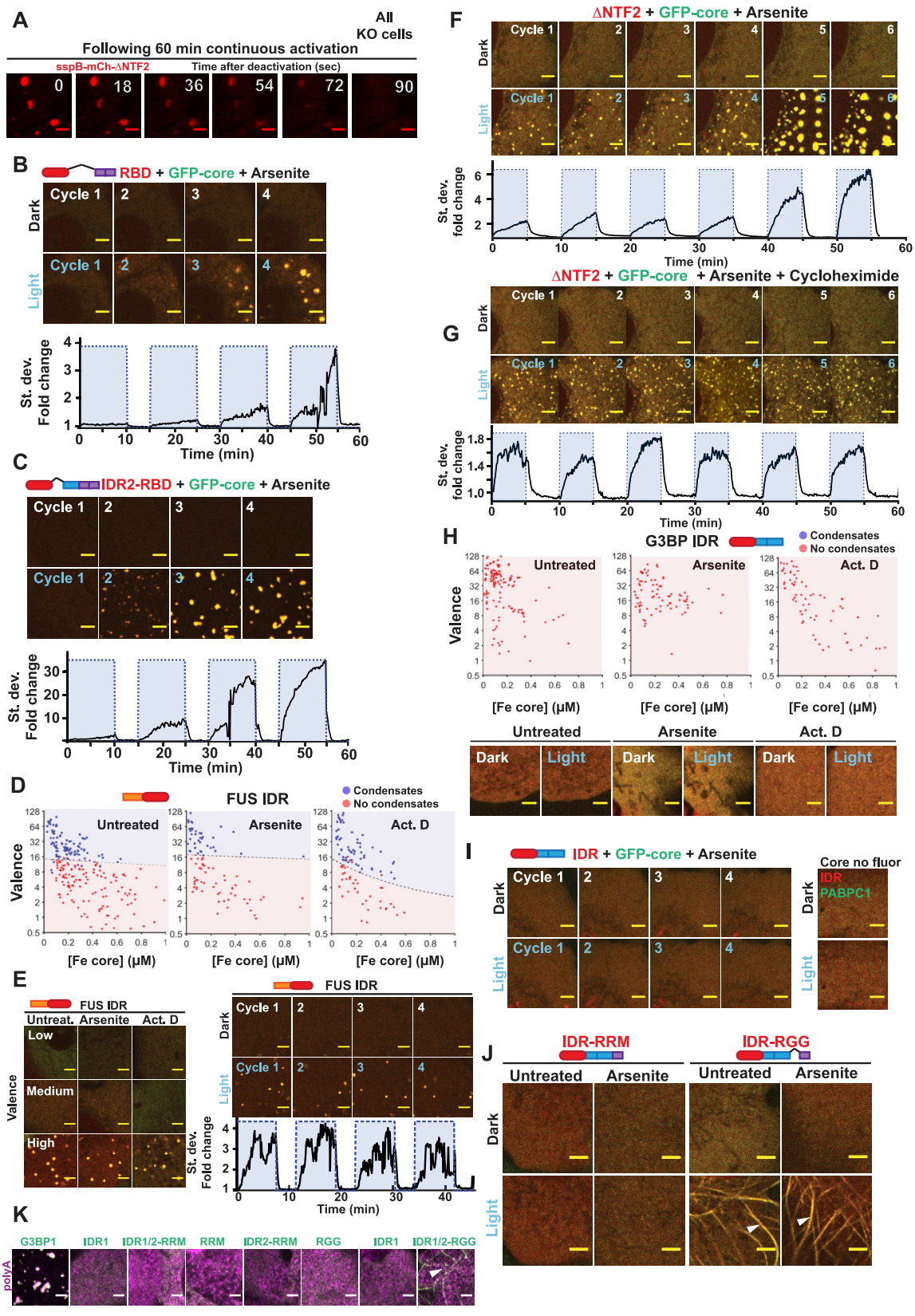

(legend on next page)

Figure S4. High-Valence G3BP RBD Complexes Are Sufficient for Stress Granule Formation with Attached P-Bodies, Related to Figure 4

(A) G3BP KO cells expressing G3BP1ΔNTF2 Corelets were As-treated and immediately activated with blue light (continuous). 1 h later, cells were deactivated (time indicated). Scale bar, 3 μm.

(B) G3BP KO cells expressing G3BP1 RBD Corelets (*v*~6-8; core~0.25 μM) were As-treated and immediately subjected to four 15-min activation-deactivation cycles (10-min on, 5-min off). Representative images shown for last frame of cycle. Scale bar, 3 μm. Bottom: standard deviation of pixel intensity relative to first image.

(C) Similar to (B) except using G3BP1 IDR2-RBD Corelets. Granules appear irregular, similar to GFP-G3BP1ΔIDR1 (see Figure 1H).

(D) G3BP KO cells expressing FUS IDR Corelets were treated with noted drug (As, 1 h; ActD, 12 h) followed by activation (5-min). Cells were assessed for LLPS and intracellular phase diagrams plotted. Each dot = separate cell (blue, LLPS; red, no LLPS). Best-fit phase threshold displayed.

(E) Left: Representative images for Figure S4D: core~0.25 μM, *v* marked (low~3, medium~6, high~18), drug treatment indicated (As, 1 h; ActD, 12 h). Scale bar, 3 μm (all images). Right: Similar to (B) except using FUS IDR Corelets (*v*~18).

(F) G3BP KO cells expressing ΔNTF2 Corelets (*v* ~18; core~0.25 μM) were As-treated and immediately subjected to six 10-min activation-deactivation cycles (5-min on, 5-min off). Representative images shown for last frame of each cycle. Scale bar, 3 μm. Bottom: standard deviation of pixel intensity relative to first image.

(G) Similar to (F) but cells were pretreated with cycloheximide (30-min) to inhibit polysome disassembly ("RNA influx").

(H) Top: Similar to (D) but using G3BP1 IDR1/2 ("IDR") Corelets. No LLPS in any cell tested (red dots). Bottom: Representative images for core~0.4 μM, *v*~18 cells treated with indicated drug (As, 1 h; ActD, 12 h). Scale bar, 3 μm.

(I) Left: similar to (B) but using G3BP1 IDR1/2 ("IDR") Corelets at *v*~24. Right: representative images of G3BP KO cells expressing IDR Corelets (core, non-fluorescent; sspB-mCh-IDR, red) and PABPC1-EYFP (SG protein, green). Following As-treatment (1 h), cells were activated (5-min): no LLPS observed, PABPC1 remains diffuse. Scale bar, 3 μm.

(J) Representative images: G3BP KO cells (+/− As) expressing indicated G3BP1 Corelets (*v*~18, core~0.4 μM) were activated for 5-min. Arrowheads: binding to microtubules. Scale bar, 3 μm.

(K) G3BP KO cells expressing indicated G3BP1 Corelets (green) were As-treated (1 h), activated (10-min), and fixed. Oligo-DT RNA FISH was performed to detect polyadenylated mRNA (magenta). FL G3BP1 Corelets (left) used as positive control. In other conditions, polyA+ mRNA is diffuse (no SGs form). Arrowheads: microtubule-binding. Scale bar, 3 μm.

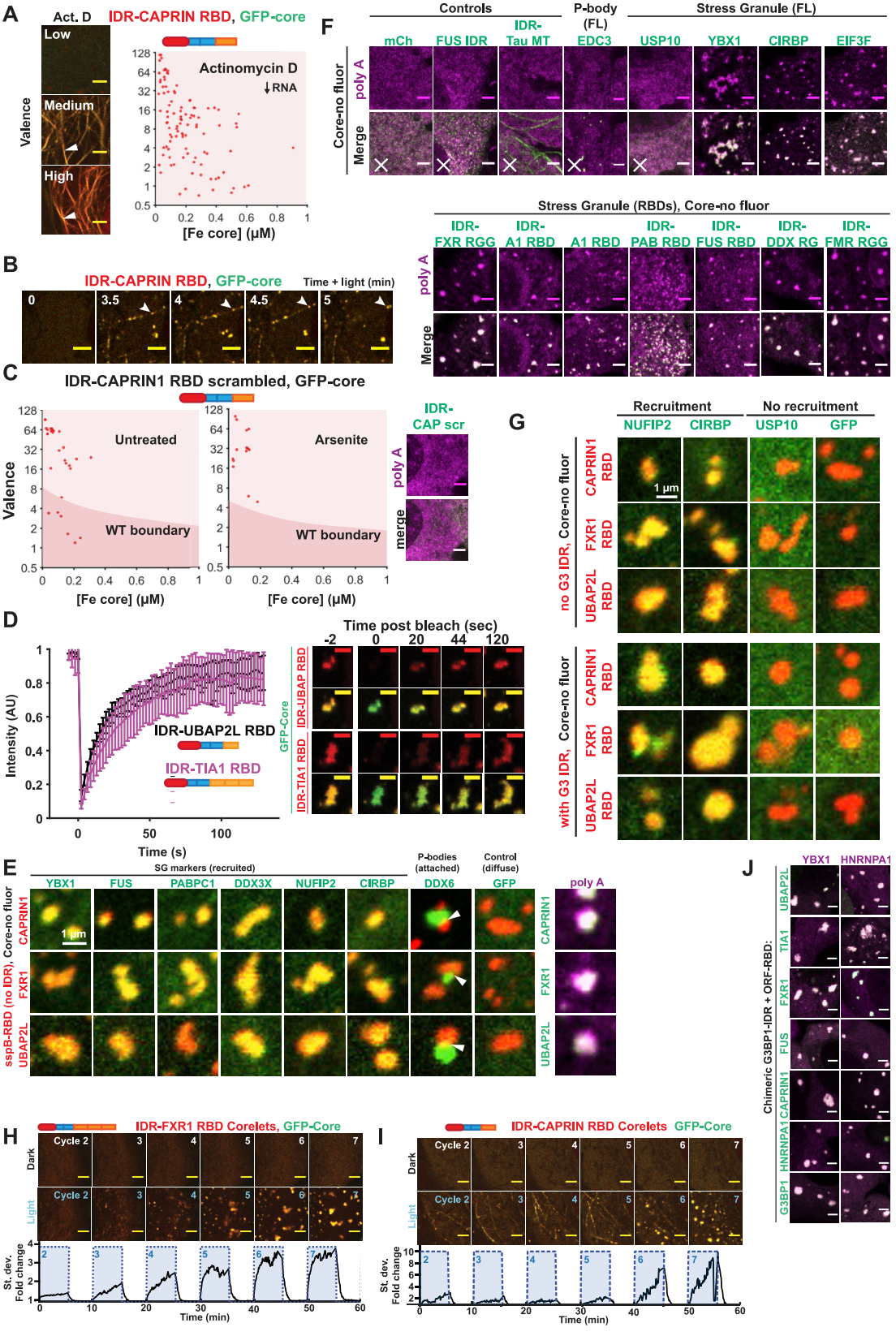

(legend on next page)

Figure S5. Stress Granules with Attached P-Bodies Are the Default Multiphase Condensate Encoded by High-Valence RBD Nodes, Related to Figure 5.

(A) G3BP KO cells expressing G3BP IDR1/2 ("IDR")-CAPRIN1 RBD Corelets were treated with ActD (12 h) and activated (5-min). Left: representative images for cells with core~0.25 μM and indicated *v* (low~3, medium~6, high~18). IDR-CAPRIN RBD Corelets bind microtubules (arrowheads). Scale bar, 3 μm. Right: intracellular phase diagram, each dot = separate cell (red, no LLPS).

(B) G3BP KO cells (no As) expressing IDR-CAPRIN1 RBD Corelets were activated (5-min). Representative images show directional movement along microtubules. Time since activation indicated. Scale bar, 3 μm.

(C) Intracellular phase diagrams for activated G3BP KO cells (+/− As) expressing IDR-CAPRIN1 RBD (scrambled) Corelets were plotted (+/− As). Non-scrambled phase threshold, shaded region (see Figure 5C). Right: As-treated cells expressing IDR-CAPRIN1 RBD (scrambled) Corelets (green) were activated (10-min) and fixed. Oligo-DT RNA FISH was performed to detect polyadenylated mRNA (magenta). Scale bar, 3 μm.

(D) G3BP KO cells expressing indicated Corelet ("IDR" = G3BP1 IDR1/2) at core ~0.25 μM and *v*~18 were As-treated (1 h) and fluorescence recovery after photobleaching (FRAP) experiments performed. Left: Granule fluorescence intensity relative to before bleach. Mean and SEM: n = 8 experiments. Right: Representative images for FRAP time course. Scale bar, 2 μm.

(E) G3BP KO cells expressing indicated Corelets (core, no fluorescent tag; sspB-mCh, red) and GFP-tagged protein (green) were As-treated (1 h), activated (10-min), and fixed. Arrowheads indicate PBs adhered to opto-SGs. Far right: similar protocol but with iLID-GFP-Fe to visualize cores (green) and oligo-dT FISH performed to detect polyadenylated RNA (magenta).

(F) G3BP KO cells expressing indicated Corelets (core, green; sspB-mCh, not shown) were As-treated (1 h), activated (10-min), and fixed. Oligo-DT RNA FISH performed to detect polyadenylated mRNA (magenta). Co-localization (white) occurs in all cases except controls, EDC3 (PB protein), and USP10 (no RBD). See Table S1 for protein domains.

(G) Similar to (E) except using different GFP-tagged proteins and RBDs with or without G3BP1 IDR1/2 ("IDR").

(H) G3BP KO cells expressing IDR-FXR1 RBD Corelets (*v*~6, core~0.25 μM) were As-treated and immediately subjected to seven 10-min activation-deactivation cycles (5-min on, 5-min off). Representative images for last frame of each cycle. Scale bar, 3 μm. Bottom: standard deviation of pixel intensity relative to first image. First cycle not shown due to space constraints.

(I) Similar to (H) but using IDR-CAPRIN1 RBD Corelets.

(J) G3BP KO cells expressing mCh-tagged SG protein (magenta) and GFP-tagged G3BP1 with swapped RBD (protein indicated in green) were As-treated (1 h) and imaged. White hue indicates co-localization (SG rescue). Scale bar, 3 μm.

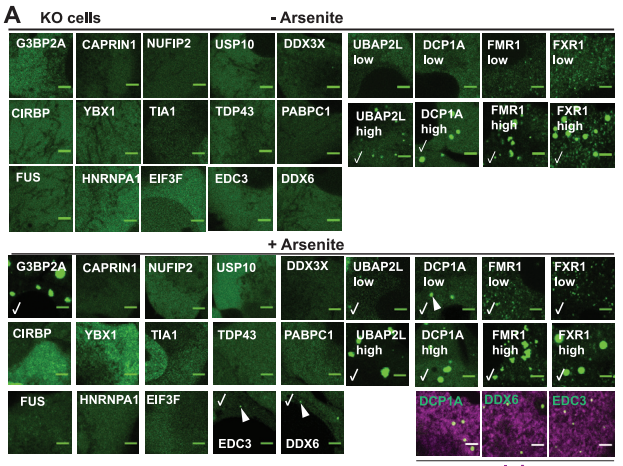

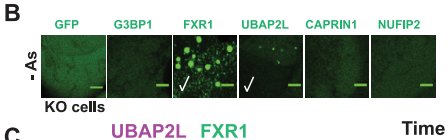

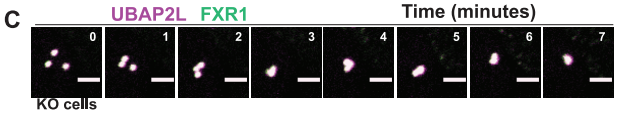

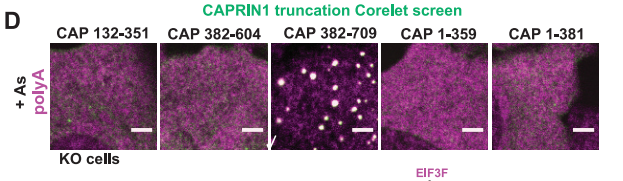

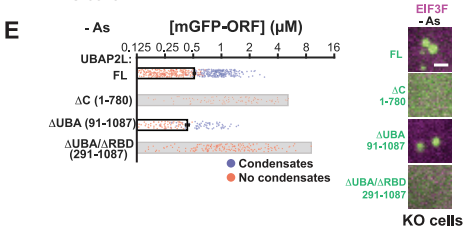

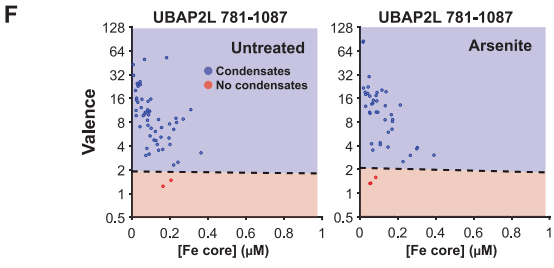

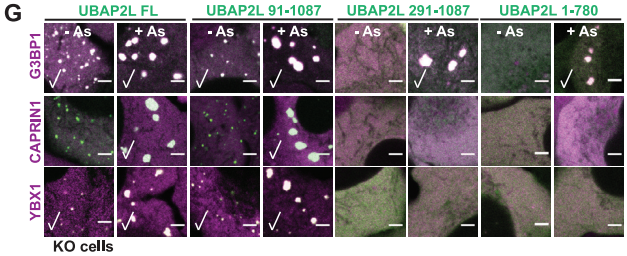

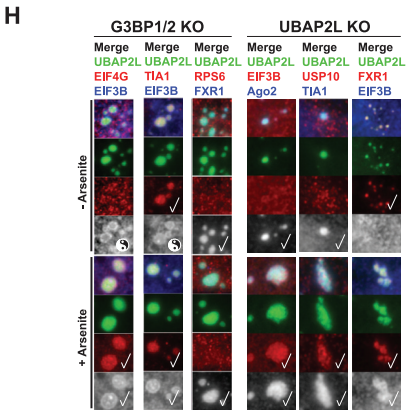

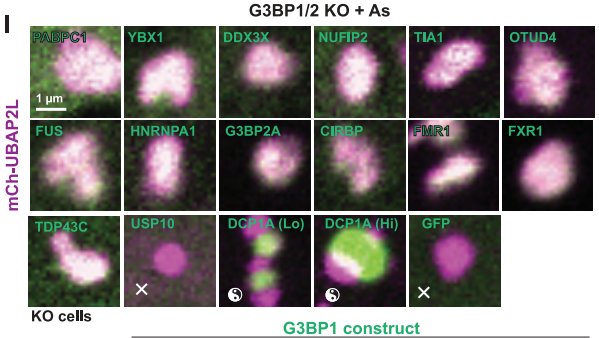

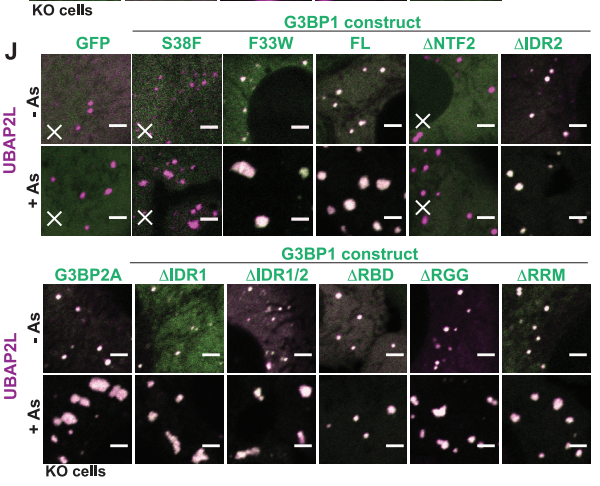

(legend on next page)

Figure S6. Competition between Protein-Protein Interaction Nodes Encodes Multiphase Condensation, Related to Figure 6

(A) G3BP KO cells expressing indicated GFP-tagged protein were assessed for LLPS (+/− As). Indicated: check, condensates (SGs or PBs); arrowhead, those found to lack polyadenylated RNA (oligo-dT RNA FISH, bottom right). Note concentration dependence of condensation in untreated cells for DCP1A, UBAP2L, FMR1, and FXR1, which is affected by As-treatment. Scale bar, 3 μm.

(B) Representative images of G3BP KO cells (no As) expressing (~1-2 μM) indicated GFP-tagged protein. Checks indicate condensates. Scale bar, 3 μm.

(C) G3BP KO cells expressing mCh-UBAP2L (magenta) and GFP-FXR1 (both ~1-2 μM) were imaged immediately following As (time since As-treatment shown). Both proteins co-localize in puncta that fuse and relax to sphere. Not shown: puncta grow in size and irregularity as available RNA increases. Scale bar, 3 μm.

(D) Representative images for CAPRIN1 fragments tested in self-associating domain screen (Figure 6C): G3BP KO cells expressing indicated Corelet were As-treated (1 h), activated (10-min), and fixed. Oligo-dT RNA FISH was performed to detect polyadenylated mRNA (magenta), which only co-localizes with CAPRIN1 382-709 (green, RBD 605-709). Scale bar, 3 μm.

(E) G3BP KO U2OS cells (no As) expressing EIF3F-mCh and indicated GFP-tagged UBAP2L were scored for condensates (EIF3F-negative). Each dot = separate cell. Mean and SEM: n = 3-4 experiments, >4 images per. UBAP2L 1-780 lacks IDR; 91-1087, UBA; 291-1087, UBA and RBD. Right: Representative images. Scale bar, 1 μm.

(F) G3BP KO cells expressing UBAP2L C terminus (781-1087) Corelets (+/− As) were activated (5-min) and assayed for LLPS. Each dot is a separate cell. Best-fit phase threshold displayed.

(G) G3BP KO U2OS cells expressing indicated mCh-tagged SG protein and GFP-tagged UBAP2L deletion protein were imaged (+/−As). Representative images shown, check = co-localization. Scale bar, 3 μm.

(H) Two-color immunofluorescence on G3BP KO or UBAP2L KO cells expressing GFP-UBAP2L (green) (+/− As). Indicated: Antibodies (with color, top); check, co-localize with UBAP2L granules; yin-yangs, multiphase bodies.

(I) G3BP KO U2OS cells expressing mCh-UBAP2L and indicated GFP-tagged protein were As-treated (1 h) and examined for co-localization. Indicated: X, no co-localization; yin-yangs, multiphase bodies.

(J) G3BP KO cells expressing mCh-UBAP2L and indicated GFP-tagged G3BP1 domain deletion/variant (+/− As). Note that S38F mutation blocks partitioning into UBAP2L granules similar to ΔNTF2 (X, no recruitment). Scale bar, 3 μm.

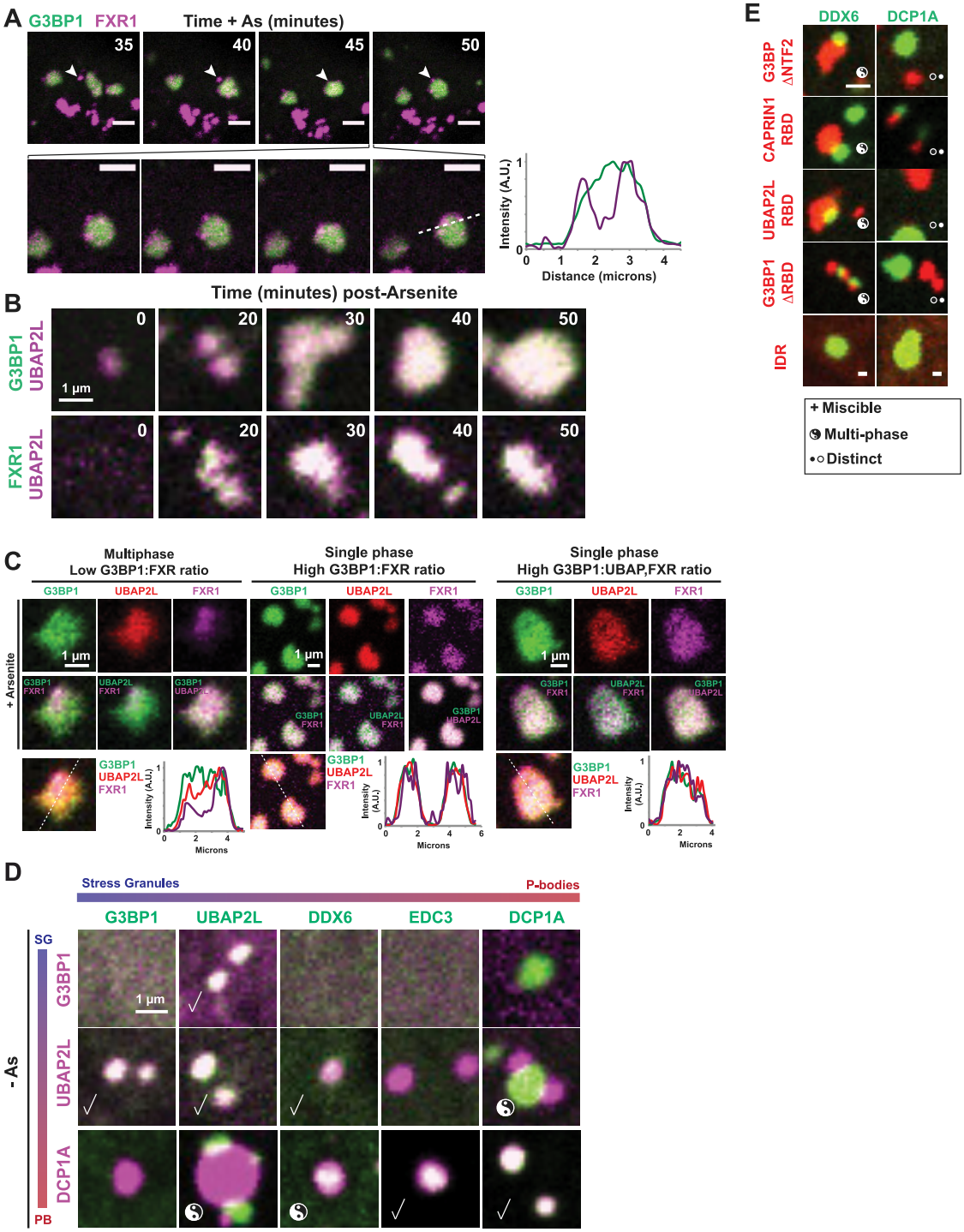

Figure S7. Competition between Protein-Protein Interaction Nodes Encodes Multiphase Condensation, Related to Figure 6

(A) G3BP KO cells expressing iRFP-FXR1 (magenta) and GFP-G3BP1 (green) were As-treated and time course performed. Arrowhead: FXR1 granules adsorbing onto surface of G3BP1 SGs. Scale bar, 3 μm. Right: Line trace profile shows multiphase coexistence within a single SG.

(B) As-treatment time courses for G3BP KO cells expressing (<2 μM) iRFP-UBAP2L (magenta) with GFP-G3BP1 (top) or GFP-FXR1 (bottom). Both pairs co-localize by confocal microscopy.

(C) Additional examples of G3BP KO triple co-expression data shown in Figure 6F. Relative concentration ratios of proteins are indicated.

(legend continued on next page)

(D) Representative images of G3BP KO cells (no As) expressing pairs of mCh- and GFP-tagged SG and PB proteins. Indicated: Checks, miscible; yin-yangs, multiphase coexistence.

(E) G3BP KO cells expressing indicated Corelet (iLID-Fe, untagged; sspB-mCh, red) and GFP-tagged protein (green) were As-treated (1 h), activated (10-min), and fixed. DCP1A expression results in PB-like condensates that dissociate from opto-SGs, similar to Figure 6K. Miscibility indicated below. Scale bar, 1 μm.